WEAR CHARACTERISATION OF FRICTION STIR PROCESSED AS21A MAGNESIUM ALLOY FOR DIFFERENT TEMPERATURE CONDITIONS

A Dissertation
Submitted in Partial fulfilment of the requirements
for the award of the Degree
of

MASTER OF TECHNOLOGY
in
PRODUCTION ENGINEERING

Submitted by:
PRASHANT DHIMAN
(2K19/PIE/17)

Under the Supervision
of

Dr. R. C. SINGH
(Professor)
Department of Mechanical Engineering,
Delhi Technological University

Dr. K. SRINIVAS
(Associate Professor)
Department of Mechanical Engineering,
Delhi Technological University

DEPARTMENT OF MECHANICAL ENGINEERING
DELHI TECHNOLOGICAL UNIVERSITY
NEW DELHI-110042, INDIA

CANDIDATE'S DECLARATION

I, Prashant Dhiman, hereby certify that the work which is being presented in this dissertation entitled "WEAR CHARACTERISATION OF FRICTION STIR PROCESSED AS21A MAGNESIUM ALLOY FOR DIFFERENT TEMPERATURE CONDITIONS" being submitted by me is an authentic record of my own work carried out under the supervision of Dr. Ramesh Chandra Singh, Professor, and Dr. K. Srinivas, Associate Professor, Department of Mechanical Engineering, Delhi Technological University, Delhi.

The matter presented in this dissertation has not been submitted in any other University/Institute for the award of M.Tech Degree.

Date: Prashant Dhiman
Place: (2K19/PIE/17)

CERTIFICATE

This is to certify that the dissertation entitled "**Wear Characterisation of Friction Stir Processed AS21A Magnesium Alloy For Different Temperature Conditions**" for the partial fulfilment of requirement for the award of the degree of **Masters of Technology in Production Engineering** submitted in the **Department of Mechanical Engineering at Delhi Technological University, Delhi**, is carried out by Prashant Dhiman, roll number- 2K19/PIE/17 during a period from July 2020 to July 2021, under our supervision.

The declaration made by Mr. Prashant Dhiman, roll number- 2K19/PIE/17 is correct to the best of our knowledge and belief.

Dr. K. Srinivas
(Associate Professor)
Department of Mechanical Engineering
Delhi Technological University

Dr. R. C. Singh
(Professor)
Department of Mechanical Engineering
Delhi Technological University

ACKNOWLEDGEMENTS

I would like to express my deep gratitude, sincere thanks and appreciation to my guides **Dr. Ramesh Chandra Singh, Professor and Dr. K. Srinivas, Associate Professor, Mechanical Engineering Department, Delhi Technological University,** for their expert guidance and continuous encouragement during all stages of the dissertation work.

I would like to extend my gratitude **to Prof. S.K. Garg, Head, Mechanical Engineering Department, Delhi Technological University,** for providing this opportunity to carry out the present dissertation work.

My sincere thank to Dr. Sumit Joshi, Assistant Professor, Maharaja Agarsen Istitute of Technology and to all the faculty and staff members of Department of Mechanical Engineering (DTU), who supported me during the entire dissertation work. I am grateful to Mr. Rajesh Bohra, Mr. Manmohan, Mr. Tekchand and Mr. Roshan for their technical and experimental support. I am thankful to their kindness and generosity shown towards me, as it helped me morally complete the dissertation before actually starting it.

Finally and most importantly, I would like to thank my family members for their help, encouragement and prayers through all these months. I dedicate my work to them.

Date: Prashant Dhiman
Place: (2K19/PIE/17)

ABSTRACT

The industry inclination towards the application of light-weight materials in automobile, aerospace and marine components can be attributed to their inbuilt characteristics like high specific strength and excellent machinability. Magnesium alloys are one of the promising light-weight materials which have shown recent widespread use in structural applications.

The present study utilised Magnesium-Aluminium-Silicon (Mg-Al-Si) category based AS21A magnesium alloy. AS21A alloy is widely recognized for high thermal resistant characteristics since it contains the thermally stable Mg_2Si second phase intermetallic compound. However, the coarse morphology of Mg_2Si precipitates makes the AS21A alloy brittle in nature thus limiting their widespread application. Therefore Microstructural modification was carried out through several surface modification techniques to achieve fine precipitates thus enhancing the strength of magnesium alloy. Friction Stir Processing (FSP) is the fast growing technology which can refine the microstructure of AS21A alloy in solid state only unlike conventional techniques. FSP is gaining its position in fabrication and manufacturing industry as most used technique because it modifies the coarse grain structure of material to fine grain microstructure that leads to better machinability, improved wear resistance and also eliminates the various casting defects present in the materials like porosity by generating homogeneous dispersion of particles.

The current study is confined to the Tribological characterization of Friction Stir Processed (FSPed) AS21A alloy consisting of fine Mg_2Si precipitates. Tribological study was carried out at 10-30 N normal loads with respective temperature conditions ranging from 50^0C – 200^0C. The wear behaviour was evaluated from Linear Reciprocating Tribometer (LRT) test rig and different conclusions were derived on the basis of results obtained, thus explaining the wear performance of FSPed AS21A alloy in elevated thermal ambient.

Keyword: Magnesium; tribology; FSP; friction stir processing; wear; Mg2Si; Mg-Al-Si

CONTENT

LIST OF FIGURES

LIST OF TABLES

Chapter-1

INTRODUCTION

Lightweight materials are great inventions for improving efficiencies and reducing the load on power transmission from the prime mover. In the modern era of automobile engineering and aerospace engineering, the most significant motives are reduction in fuel consumption and to follow the intrinsic international norms of environment. Most of the automobiles consume fuels based on fossil products. Fossil fuel is depleting day by day and the scientists are working on saving of the energy or using alternative methods of energy. One and foremost way is to use lightweight alloys for the process of fabrication and manufacturing and for that magnesium alloys have proved themselves of greater use [1].

Apart from that, environment-friendly vehicles are of great concern as of today's pollution is concerned; environment protection agencies have suggested that lighter vehicles will consume less fuel and that will result in less carbon emission.

They have also suggested that if we reduce 10% weight of the vehicle, then that can lead to 6% - 8% less fuel consumption, and as a result, a lightweight vehicle will emit less pollution and can be a part of the race of environment protection [2].

Therefore, lightweight alloys are in current demand and a lot of research to make lightweight alloys useful is going on. Aluminium alloys were the most used alloy but after the processing on magnesium it has become a worthy material for fabrication purposes because of its better mechanical properties at elevated temperatures.

1.1. Material:

Magnesium is one of the most available structural materials used that has vast range of applications. But, it is not used in its pure form; rather, it is alloyed with other elements to improve its multiple properties so that it can have further applications [3].

Physical properties of the magnesium and its alloys due to which it has vast applications are presented in Table-1.1.

Table- 1.1 Properties and applications of Magnesium

Property	Application
Low density (1.7gm/cm^3)	Structural Materials
High Tensile Strength (Yield: 130MPa)	Aerospace and Automobile Applications
Better Castability	High Pressure Die Casting
Better Machinability (Lower Value hardness)	Turning and Milling at High Speeds

But these above properties are limited at elevated temperatures [4]. Some of the physical properties of the magnesium are that it has silvery white appearance, divalent metal with atomic mass of 24.305 and in pure-metal conditions at 20^{o}C, its specific gravity is 1.738 and 0.32nm is the atomic diameter of magnesium.

The structure of grain is the main criteria for defining various characteristics of the material, and casted magnesium doesn’t show fine grain structure. Therefore, the strength shown by the magnesium alloys is not as high strength as expected from them. Thus, various other elements like aluminium, titanium, zirconium, etc. are alloyed with magnesium so that their grain refinement can take place and results in improvement of different characteristics of the material [5].

Alloying of any material is very important as every material has its significant characteristic value and it adds up new characteristic feature to the parent material as some of the commonly used alloying materials [4,8].

1.2. AS21A Magnesium Alloy

Magnesium series of Silicon alloy has unique characteristics of temperature resistance along with other mechanical and wear properties that magnesium alloys have. The physical properties of the Mg_2Si particles are shown in Table:1.2. The presence of silicon in the magnesium allows to enhance the fluidity of the alloy that further enhances the casting ability of the material and can have less casting defects comparatively.

The presence of Mg_2Si in the Magnesium alloy allows it have high temperature characteristics as the melting point of Mg_2Si intermetallic is about 1100^{o}C. Better creep resistance, better heat resistant with high potential and lightweight Silicon based magnesium alloys are already used in automobile applications and also increasing their use in aerospace applications day by day [9].

The particles of Mg_2Si have found their importance in the magnesium alloy because of following properties [11]:

Table-1.2 Properties of Mg_2Si Particles

	Property	Value
1.	High value of Melting Point	1358 K
2.	Low value of Density	2×10^3 kg/m^3
3.	High value of Hardness	460 HV
4.	Low value of Thermal Expansion-Coefficient	7.50×10^{-6} K^{-1}
5.	High value of Modulus	120 GPa

The compound of Mg_2Si is dark blue in colour and solidifies in Face Centred Cubic structure [12]. The structure of Mg_2Si is found to be coarse and granular due to dendritic solidification [10]. The limitation of Mg_2Si in Magnesium Silicon alloy is that it forms the shape of Chinese script and granular phases of Mg_2Si; and lower rate of solidification is observed due to eutectic-reaction, resulting in poor mechanical characteristics of magnesium alloys. This leads to a limit in applications of these alloys.

Therefore, to remodel the phases, different types of surface modification techniques are employed such as rapid-solidification, hot-extrusion, micro-alloying, etc. [13].

Moreover, these techniques are able to modify the grain structure of the materials alloy and improving the mechanical characteristics, especially ductility. But these techniques are quite conventional in nature which obstructs the grain refinement up-to certain values.

Therefore, for better dispersion of particles and fine grain refinement some other latest methodologies are used such as Severe-Plastic-Deformation methods like Equal-Channel-Angular-Pressing technique [14], High-Pressure-Torsion technique [15], Cyclic-Extrusion-Compression technique [16], Repetitive-Upsetting-Extrusion techniques [17], Cyclic-Closed-Die-Forging technique [18], Friction-Stir-Processing technique [19] etc. These methods of grain refinement are used in various lightweight alloys and these methods have shown greater results. There are a lot of recent studies going on these methods to take more out of these methods and fulfil the demands of the cutting-edge technologies [14-19].

1.3. Friction-Stir-Processing Technique (FSP)

Friction-Stir-Processing is a new technique that is gaining attention that modifies the characteristics of the material through the process of plastic deformation of localized area and this is not only efficient in saving energy but also friendly with environment as generally no harmful fumes are generated [20].

This processing method is based on the principle of the Friction Stir Welding Process and is being utilised for surface modification by the modification of microstructures of the materials.

In order to produce better mechanical properties in the material sheets, this technique is showing its full potential in doing so. Also, from last decade a lot of research is going on to improve various machining processes and Friction Stir Processing is gaining attention from round the world as a latest and improved technique for modifications in microstructures of the material with high level of efficiency [21].

Friction Stir Processing benefits the material properties in many ways. It is used in mixing two metals (or materials); that is, it is used for making alloys apart from that stirring of individual material leads to modifying the grain structures. This processing technique performs in a solid-state, and no melting of the metals takes place to complete the Friction Stir Processing technique; and in solid-state only, uniform mixing of two materials takes place, and generated material has better mechanical characteristics as compared to unprocessed material of the same type [20].

1.3.1. **Applications of FSP**:

Casting	Casting produces materials that have different casting defects like porosity, and other defects like cold flakes in microstructure; still casting is utilised for vast applications because it is quite an economical process. Therefore, to improve the surface properties and to remove these defects by developing homogeneity in the materials

	and modifying the grain structure with the help of Friction Stir Processing [22].
Powder Metallurgy	Friction Stir Processing enhances the microstructural characteristics of materials produced by powder metallurgy, which has improved the mechanical properties like hardness, ductility, toughness, etc. because of the application of Friction Stir Processing for localized treatment of the materials [23, 24].
Metal Matrix Composites	Friction Stir Processing techniques are utilised to fabricate or manufacture metal matrix composites which are having improved thermal conductivity, better grain structure and other mechanical properties like toughness, ductility, and also other tribological characteristics. [25,26,27].

1.3.2. **Working Principle:**

In general, Friction Stir Processing works alike Friction Stir Welding and based on thermomechanical technique in which, at elevated temperatures, plastic deformation in the material takes place, normally temperature is approximately about 0.5 times of melting point of the material [28].

The working principle of Friction Stir Processing is quite simple as a non-consumable, specially developed tool is allowed to rotate at sufficient speeds and also a downward push is applied in order to penetrate the tool into the surface of the material and then a linear motion is also provided that allows tool to travel from one end of the specimen to the other as shown in Fig: 1.1.

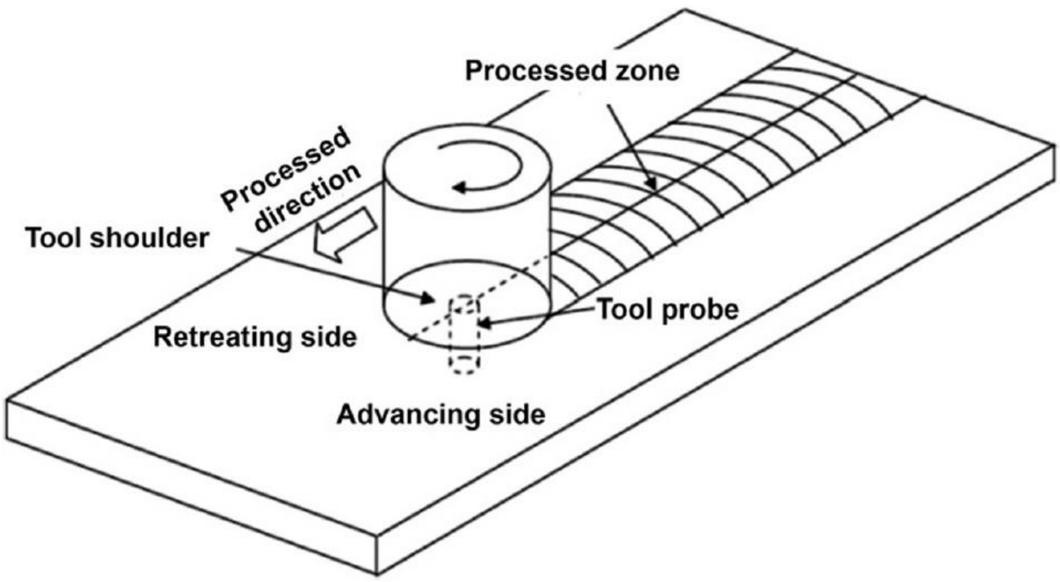

Fig: 1.1 Schematic description of FSP [20]

The rotating tool produces a considerable amount of heat in the material near tool and raises the temperature in the material that is favourable to the plastic deformation and then as the tool covers linear path into the material with a defined speed. The area near the pin is plastically deformed and the tool is moving ahead by producing processed region in the material.

The edge of the tool, leading in the material also produces a forging action in the downward direction because of the fact that the tool is given a tilt angle to support the action and the tilt angle generally ranges from one to three degrees of angle [28,29].

The process also generates different zones or regions in the material after the processing and these zones are categorized as Stir Zone, Thermo-mechanically Affected Zone (TMAZ) and Heat Affected Zone (HAZ) as shown in Fig: 1.2. The size and properties of these zones entirely depend on the different process parameters of the tool like the rotating velocity of the tool, transverse velocity of the tool, profile of the pin of the tool, depth of penetration in the material, thickness of material plate, thermal conductivity, etc. [20,29].

The zone which bears the maximum temperature as well as maximum strain is the region known as Stir Zone. This region also undergoes the maximum value of grain refinement. The various dimension of stir zone like the depth, width and the volume of the zone is defined by the parameters of the tool like the length of the pin measures the depth of the zone and the diameter of the shoulder determines the width of the zone [20,29].

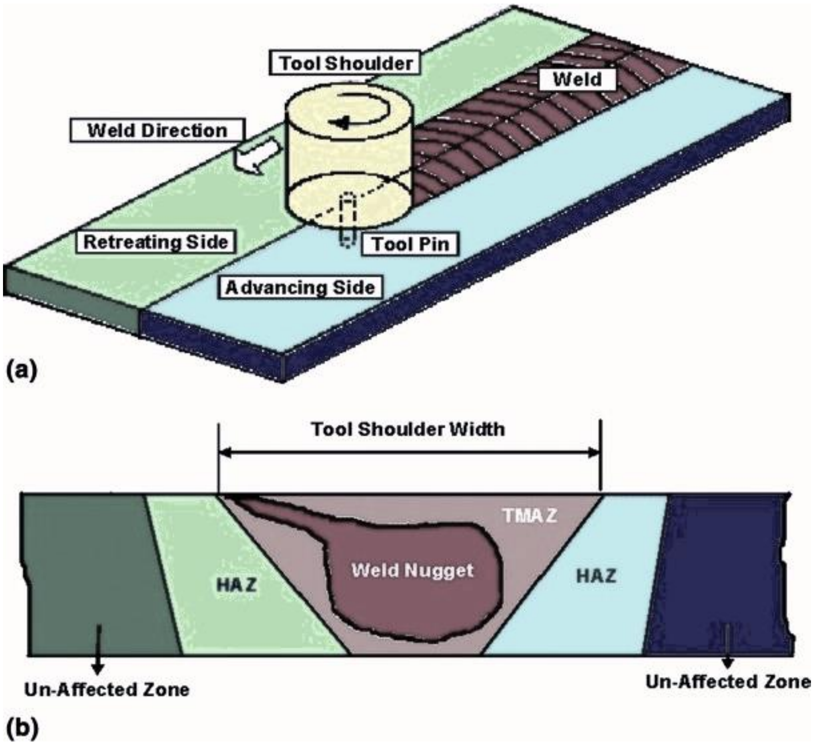

Fig: 1.2 Different zones and terminologies present in Friction Stir Processing [28]

Thermo-Mechanically Affected Zone (TMAZ), this zone ranges from few micrometres to millimetres in size and undergoes lower heat generation than that of stir zone and no recrystallization takes place in this zone as the value of strain rate is quite low for recrystallization. The width of this zone totally depends on the material property if a material is soft like Aluminium, magnesium then the width of the zone is quite large as compared to the width that forms in the case of hard materials like titanium and steels [29].

Heat Affected Zone (HAZ), this zone lies between Thermo-mechanically affected zone and the parent material on which processing is done. There is hardly any strain in this zone and thermal cycles are observed here, that results in grain growth. Therefore, the size of grain in this region is comparatively bigger in size as compared to that of parent material. The mechanical properties in this zone are also relatively poor and while performing tensile test then failure will take place in this zone [29,30].

1.3.3. **Process Parameters:**

The process parameters have always the great influence on any machining process or it is the only factor that has to be dealt carefully while performing any operation. Here, in the case of Friction Stir Processing, process parameters are distributed in the following categories as Parameters of Tool, Parameters of Machine and Particle Parameters.

1.3.3.1. Tool Parameters:

The tool in the Friction Stir Processing is comprised of two parts, one is Pin and other is Shoulder. While performing the operation, both of the components are very important in order to generate heating in the material and the flow of the plastically deformed material [33]. Fig: 1.3 shows the parameters of the tool that affect the properties of the processed material.

The tool pin profile plays an important part and it can vary differently as per the applications. The profile of pin can be triangle, square, cylindrical. Apart from that profile can be threaded, fluted and conical, different profile has different advantages, therefore, the profile of the pin is selected as per the need of the processing. [32,33].

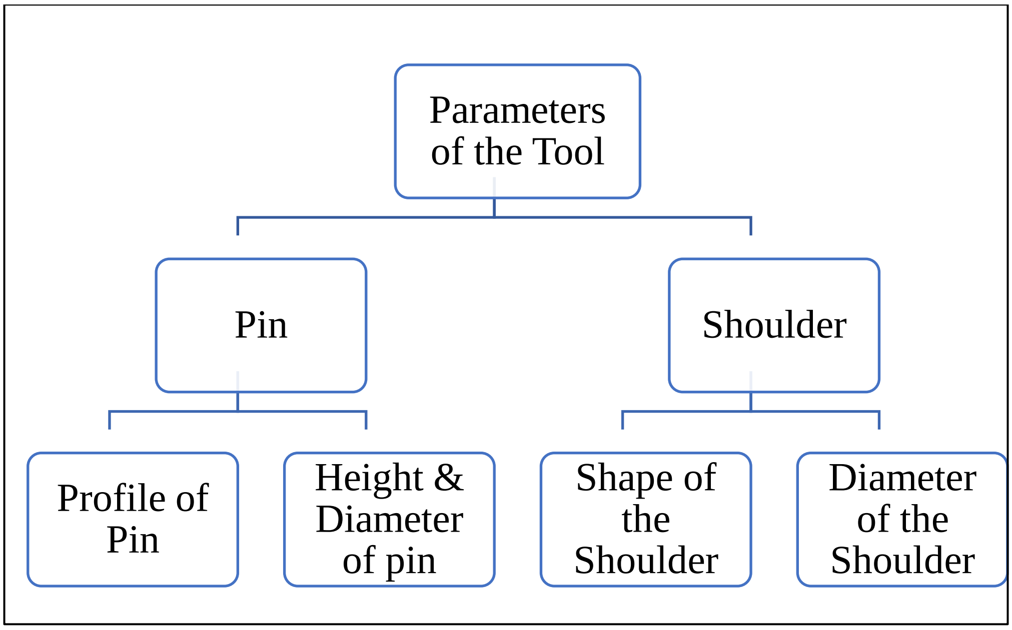

Fig: 1.3 Categorization based on the Tool parameters [34]

1.3.3.2. Parameters of Machine:

There are various machine parameters that leads to the performance of the Friction Stir Processing and these are shown in Fig: 1.4. The number of passes, speed of the rotation and the travel speed of the tool are important parameters. These parameters affect majorly on the outcome of the process, mostly affected are microstructures of the material and amount of heat generated in the material.

If the speed of rotation increases, the stirring of the material in the sample will take place more rigorously. This will result in increase in the temperature of the area and if simultaneously the travel speed of the tool decreases, means tool will spend longer time at a place that will result in more heat generation in the vicinity and accordingly the grain growth will take place [29, 35].

Therefore, the ratio of rotational speed to traverse speed will decide the grain structure. The higher values of the ratio will generate coarse grains as generation of heat is high and lower values of the ratio will generate finer grain structure [35,36].

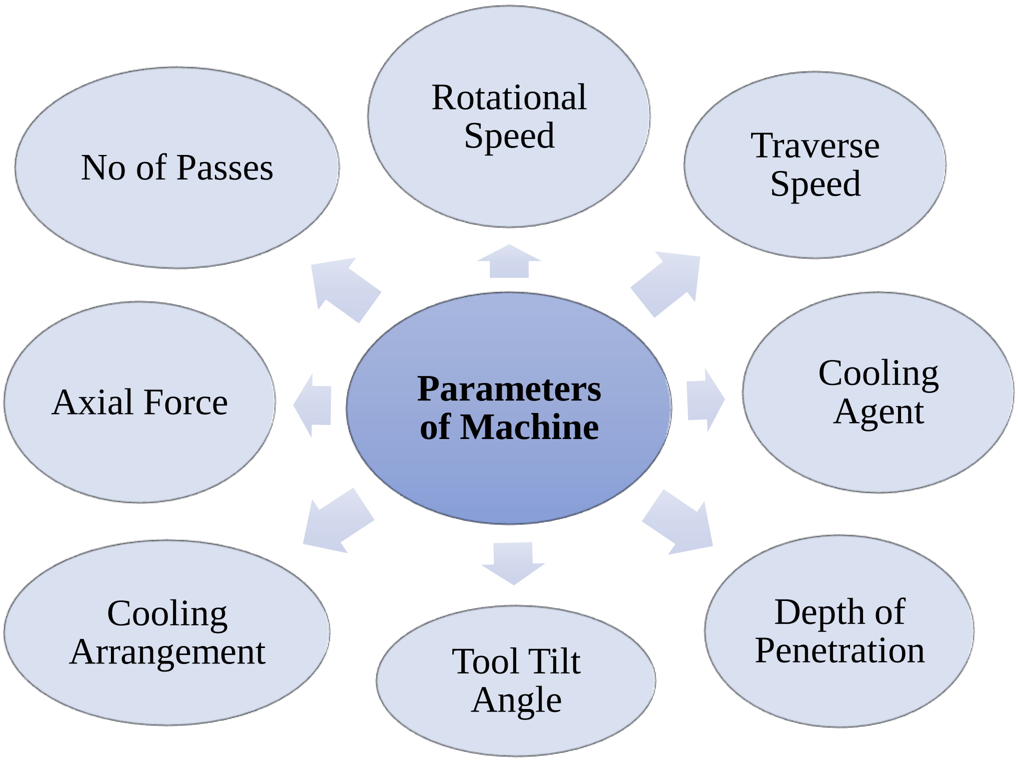

Fig: 1.4 Parameters of Machine for Friction Stir Processing [34]

1.4. Wear:

There are different ways in which material degradation takes place, like corrosion, wear and due to ultraviolet light, specific degradation of polymers. This material degradation leads to a material loss in the sample [37].

Take any case in which the surface of a hard material X is in contact (say sliding) with a soft material surface Y, then the wear for the same will be:

$$\frac{V}{L} = K\frac{F_n}{H} \quad \text{….. (1.1)}$$

Here,

- V- Volume of the metal removed
- L- distance of sliding by X or Y
- F_n- Normal Load
- K- Wear Coefficient

Some of the ways used to quantify wear are as follows:

(a) Analysing the weight of the tested samples carefully
(b) Analysing the metal removal volume with the help of 3-D tools.
(c) If lubricants are used, then filtration of oils and the measurement of wear debris in the lubricants should be done carefully.

Wear can be classified into various categories, but majorly we study four types of wear, namely Adhesive, Abrasive, Fatigue, Tribochemical and Fretting Wear [37].

1.4.1. Adhesive Wear:

When surfaces are subjected to friction, then small junctions or micro-welds can be observed on the surface, this wear is characterised as adhesive wear and shown in Fig:1.5 (a).

If the junctions observed are weak, then due to shear, these can be removed on their own, but if these are strong, then they got transfer from soft material to hard material causing a material loss in soft materials [37,38].

1.4.2. Abrasive Wear:

Abrasive wear (shown in Fig:1.5 (b)) is observed in surface interaction of hard materials and comparatively softer materials. We can observe wear grooves and scratches on the surfaces that results in material removal; further causing material loss [39].

1.4.3. Fatigue Wear:

Fatigue wear is generally caused by the Cyclic Loads, and these loads induce strain in the layers of surface materials. Fig: 1.5 (c) depicts the nature of Fatigue wear. This results in formation of cracks in the material and simultaneously their development leads to the formation of debris that looks like a flake and new name of the wear is introduced that is delamination wear [40].

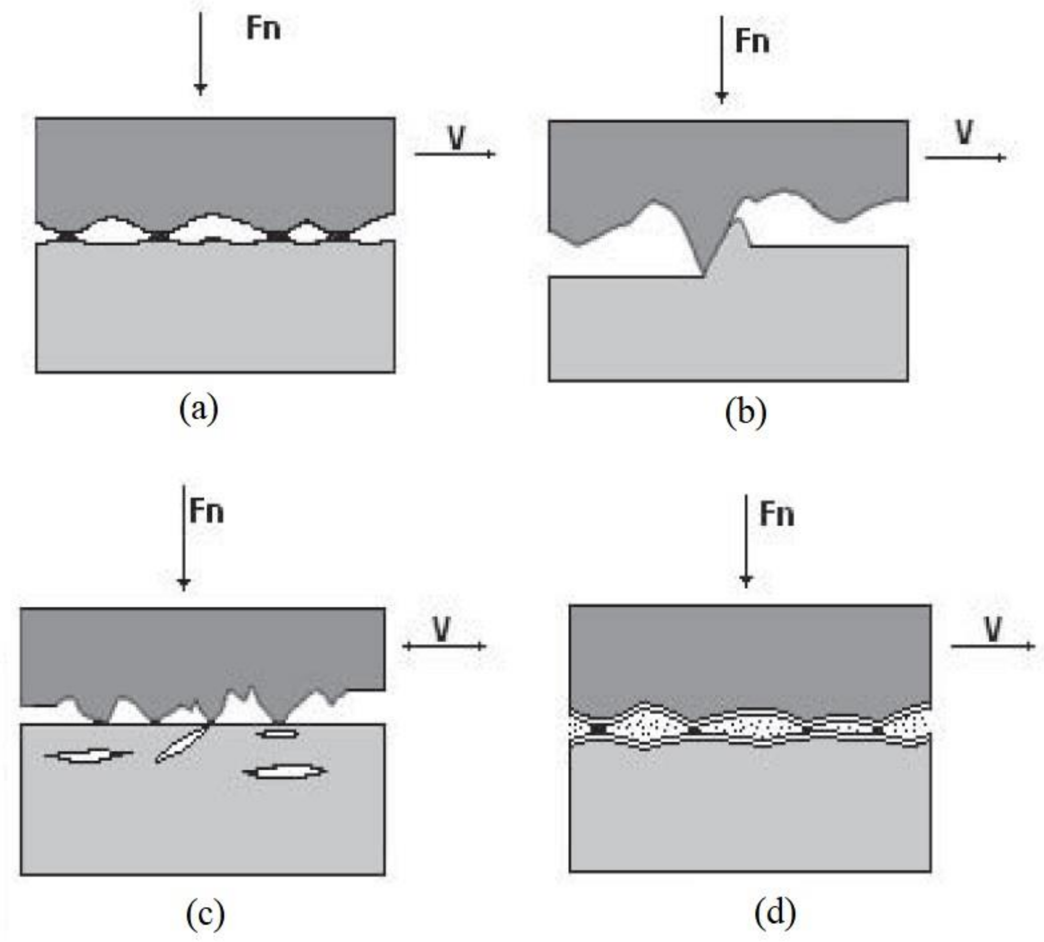

Fig: 1.5 Description of different wear forms [37]

1.4.4. Tribochemical Wear:

Tribochemical Wear shown in Fig: 1.5 (d). It is a phenomena in which the interaction of two mating surfaces (or contacting surfaces or interaction with the surroundings) leads to a chemical reaction on the surface. A film of reaction products develops on the surface, for examples, tribo-oxidation wear.

As friction increases, it increases the temperature of the interface that increases the rate of growth of oxide film on the surface. This film can be separated from the surface if it has attained some thickness [37].

1.4.5. Fretting Wear:

Fretting Wear takes place when the contacting surfaces are either moving in reciprocating motion or in an oscillating motion. The amplitude of the oscillation is relatively small.

Fretting Wear is a multi-step mechanism in which during solid-state contact, initially, adhesive wear is observed due to rubbing between solid surfaces and this leads to debris at the interface. Then oxidation of this debris takes place in the surrounding environment and leads to storage of energy in this debris. Since these particles are highly likely to oxide heavily and rapidly, it leads to a large number of debris present on the surface [41].

Chapter-2

LITERATURE REVIEW

The literature review has been carried out in different sections before conclusion of literature gap and research objective of the study. Firstly, the morphological study of Mg_2Si has been covered and wear behaviour of Magnesium-Silicon alloy. Secondly, the literature review is carried out about new surface modification techniques that enhance the mechanical and wear properties of different light weight alloys.

2.1. Morphology of Mg_2Si

Reference	**Processing Method**	**Material**	**Results**
Kim et al. [42]	Squeeze Casting	Mg-5Al-1Zn-0.7Si Addition of 0.2% Ca and 0.03% P.	Modification of Chinese script Mg_2Si particles into polygon type Mg_2Si particles by the addition of Ca and P. That results in removal of nucleation sites which leads to the improvement in toughness and tensile properties.
Guo et al. [43]	Gravity Casting	Mg-Si Alloy Addition of 0.5% Bi and 0.8% Bi.	Adding an optimum amount (i.e. 0.5%) of Bi in Mg-5Si alloy produces a fine grain structure of polyhedral shape from a coarse dendritic form of Mg_2Si. Even the size of Mg_2Si was reduced to 15µm or less.
Wang et al. [44]	Casting	Mg-Si alloy with K_2TiF_6, KBF_4 and KBF_4 + K_2TiF_6	5% K_2TiF_6 is added, and no significant changes were observed, whereas, when 5% KBF_4 is added to Mg-5Si alloy melt, the particle size of Mg_2Si has reduced to 20µm or less.

			Moreover, adding 5% KBF + K_2TiF_6 (in a 4:1 ratio) has changed it back to an irregular shape and coarser grain structure again.
Qin et al. [45]	Casting and aging treatment	The in-situ composite of Al-25 Mg_2Si-3Si-3Cu-0.5P	Modified composite has increased Tensile strength by 31.1% and elongation by 1.345%, which showed improvement in Tensile Strength and Plasticity. The size of Mg_2Si particles is modified from dendrite to polygon and reduced to an approximate size of 20um.
Xiong et al. [46]	Powder Metallurgy, Ball Milling, Reactive Hot-Pressing	Mg- 150µm and Si- 150 µm Powders	With increase in Ball-to-Powder Mass Ratio, there is decrease in grain size of Mg and Si. Fracture hardness and Vickers Toughness of Mg_2Si is better than that of parent material.
Qin et al. [47]	Casting	The in-situ composite Al-25Mg_2Si-3Si-3Cu-0.5P	Fine polygonal shape particles of 20µm to 50µm in size of Mg_2Si were obtained after adding phosphorus to the Al-Si master alloy. Also, it has shown the change of Mg_2Si morphology from dendritic crystal to tetrakaidecahedron, which was earlier in long fibriform and later changed to short fibriform or dot-like in eutectic Mg_2Si phases.

Bo et al. [48]	Casting	20 Mg_2Si/ Al-5Si Composite. The Mg and Al-3Sb were mixed into the Al-Si melt.	0, 0.2, 0.4 and 0.6 by percentage mass fraction of Sb is added. The optimum value of 0.4 by percentage mass fraction of Sb shows that the primary structure of Mg2Si was changed to fine particles of the approximate size of 25um. An improvement of ~35% in Ultimate Tensile Strength and ~38% in elongation was observed, which has resulted in high resistance to cracks.
Ahlatchi [49]	Hot Extrusion at 300^{o}C	Al-12 Si – X Mg Alloys (0% to 20% weight variation in the content of Mg)	Compression Strength and Hardness of the alloys are improved by the addition of Mg. By the process of Hot-Extrusion the Chinese script particles of Mg_2Si is modified to needle shaped fine particles.
Hadian et al. [50]	Casting	Al- 15% Mg_2Si Composite	0.3% of Li addition has shown the refinement of grain structure and reduces the size of the structure from 30 µm to approximately 6µm. Also, the increased cooling rate and the addition of Li has increase the Ultimate Tensile Strength and Elongation values.
Qin et al. [51]	Melt Superheating and Casting	Mg_2Si / Al – Si – Cu Composite	Size of Mg_2Si particles modifies to equiaxed from coarse dendritic and also the size is

			decreased from 150µm to approx. 50-40 µm. Chinese script type of eutectic Mg_2Si changes to needle like structure.
Liao et al. [52]	Casting and Ageing Treatment	Mg_2Si / Mg – 9 Al – Sb Composite	By the addition of 0.5 Wt.% Sb. The particle of Mg_2Si is modified, refined and reduced in size also change from Chinese script type to polygonal shape. Further improvement in tensile strength, elongation and damping capacity; also, the value of critical strain amplitude is decreased and improvement is noticed.
Zhang et al. [53]	Reciprocating Extrusion and Homogenization Heat Treatment	Mg_2Si / Mg – Al Composite	Before the extrusion; coarse α – Mg dendrites are present. After the twelfth pass of extrusion, Mg_2Si phases are uniformly distributed and almost are equiaxed and attain the size less than 20µm. Mechanical properties like Tensile and Yield Strength are improved the value of elongation has also increased at room temperature and some improvement at elevated temperatures.
Gan et al. [54]	Equal Channel Angular Pressing by an	3.2 Wt% of Si. The in-situ composite of	The refinement of type-II Mg_2Si is found efficiently done also

	internal angle of 90° with horizontal and vertical channels	Mg_2Si Composite	homogeneous distribution in the matrix. Yield tensile Strength along with elongation to failure value are enhance by the ECAP due to the grain refinement and homogenization of the particles. With each processing pass, the improvement in strain hardening behaviour is observed.
Wei et al. [55]	Repetitive Upsetting Extrusion	AZ 31 Mg Alloy (Mg – 3Al – 1Zn – 0.4Zn)	With each pass of Repetitive Upsetting, deformation is getting uniform. When five passes are completed, Chinese script and large dendritic Mg_2Si particles are changed to fine particles with homogeneous redistribution. A notable improvement is observed in the ductility and strength of the composite.
Metayer et al. [56]	Cyclic Closed Die Forging Process	Mg – *x* Si Alloys	Refinement of structure and homogeneous distribution is obtained after optimum number of passes. The improvement in various mechanical properties like strength, ductility and hardness is observed as a product of refinement of grain structure. Decrement in wear loss is also observed and hence better wear resistance is there.

Syukron et al. [57]	Equal Channel Angular Pressing with an internal angle of 120^o	Al – Mg – Si Alloy Adding Hard Particle TiB_2	With addition of TiB_2, the hardness of the alloy is observed to be doubled as compared to the original value. Grain refinement in the specimen if found to be modifies from 35 µm to 0.79 µm and of almost uniform size.
Chegini et al. [58]	Equal Channel Angular Processing. For four hours at a temperature of 500^{o}C, Thermal Homogenizing.	Al – $x$$Mg_2Si$ Composites	Processed sample has high strength as the sample is work-hardened and also have fine grain structure because of homogeneous distribution of Mg_2Si particle which are broken into small pieces. Around 35% Ultimate Shear Strength and around 80% Ultimate Tensile Strength has increased in processed samples. 65% and 150% increment is seen in the shear yield and tensile of the processed samples. Whereas, increasing the content of Mg_2Si and the number of passes has shown that brittle name of the specimen is increased and catastrophic cracks are formed at this parameter.
Guo et al. [59]	Cyclic Extrusion Compression	Mg – SiC nanocomposite	After eight passes of Cyclic Extrusion Compression process, large particles are fragmented

			into smaller ones and are uniformly distributed. Also, homogeneous and fine grain structure is obtained after the passes. Hardness of the sample is found to be increased after the process which is a result of fine grain particles.
El-Garhy et al. [60]	Cyclic Extrusion Compression	Al 6061 and Al 6061/SiC Metal Matrix Composites	When the number of cycles increase then increase in grain refinement and porosity reduction in the alloy takes place.
Sha et al. [73]	High Pressure Torsion	Al-Si-Mg Alloy (AA6060 alloy)	Grain refinement in the alloy, strengthening from dislocations and solute nanostructures; altogether has allowed the parent alloy to achieve high strength. The temperature range of High-Pressure torsion processing is between 100^{o}C to 180^{o}C, where less than 20 per cent of solute atoms at 100^{o}C and 85 per cent of solute atoms at 180^{o}C were observed in the processed sample.

Initially, the microstructure of Magnesium- Silicon Alloys consisted of Chinese script type of Mg_2Si particles. These particles are of a coarse dendritic shape and were sometimes found to be the equiaxed dendritic structural shape. To improve the morphology of these particles, a lot of different elements like 0.2 wt% Ca, 0.03 wt% P, 0.5 wt% Bi, 0.3 wt% Li, 0.5 wt% Sb, etc. were added to Magnesium alloys or their melts with other elements or compounds or sometimes to in-situ composites of Al-Si or Mg-Si alloys.

The addition, as mentioned earlier, of elements takes place at different levels like during gravity die casting, squeeze casting, powder metallurgy, reciprocating extrusion, superheating treatment, ageing treatment, and so on. After the addition of the elements mentioned above, there were a few improvements that were observed, such as the grains structure of Mg_2Si particles has reduced in size (approximately 15µm - 30µm), and the shape has changed to a more regular and polyhedral. Sometimes it has changed to short fibriform or dot-like from a long fibriform type of particle shape.

The significant advantage of improved morphology of Mg_2Si particles was better mechanical properties compared to its parent composite. Most improvements were noted in tensile strength, yield strength, plasticity (as elongation percentage has increased), high resistance to crack hardness, and compression strength.

Reference	**Material**	**Results**
Charit et al. [61], Kwon et al. [62] and Sharma et al. [63]	Al 2024 Hot rolled plates Al 1050 Cold rolled plates A 356 Sand Casted plates	Improvement in mechanical properties has been observed as Charit et al. [61] noticed the improvement in ductility with the relation to temperature. During the process as at 430^{o}C maximum value of elongation has been obtained whereas Kwon et al. [62] has made the observation on the basis of rotation speed of the tool and notice at 560 rpm maximum value of hardness and tension is obtained. Kwon et al. [62] has also notified that advancing side is having better results as compared to retreating side of the parent material. However, Sharma et al. [63] clarifies that there is increase in fatigue properties and crack growth can also be reduced using the technique. The casting defects like

		porosity has been removed that was the significant reason in improving the length of crack that leads to reduction in crack growth rate. All of them specified the reason that homogeneity or uniform distribution of particles and grain refinement by the Friction Stir Processing.
Sharma et al. [63], Santella et al. [64] And Ma et al. [65]	Sand Casted ingots of A 356 and A 319 alloy. Sand casted billets further converted into plates of A 356 alloy.	By the friction stir process, various defects such as porosity and the dendritic microstructures in casting are improved. Also, noticed that uniform distribution of particles has been achieved and due to which various mechanical properties are improved like ductility, tensile strength and fatigue. In order to increase the tensile strength, it has been observed that ductility plays an important role as ductility increases it leads to increase various other properties. Microstructure refinement was the reason for the improvement in ductility as porosity due to casting is removed by FSP. Grain size of approximately 3μm to 4μm has been observed after the process of FSP by Ma et al. [65] which plays significant role in redistribution and modification in size of the particles in the material at optimum parameters of the machine.
Cavaliere et al. [66] and Kang et al. [67]	Sheets of AM 60 magnesium alloys. Sheets of Al 5052 – H32 alloy	Aftereffect of the stirring action by FSP has shown the eradication of casting defects and improvement in mechanical properties.

		Cavaliere et al. [66] has shown that FSP of AM 60 magnesium alloy sheets leads to enhanced tensile properties in ambient conditions whereas Al 5052 – H32 alloy sheets after FSP has shown a considerable improvement in the formability due to fine grain structure development in processed zone of the material.
Charit and Mishra [68], Chang et al. [69] And Ni et al. [70]	Plates of Al-Zn-Mg-Sc alloy, Mg-Al-Zn or AZ31 Mg alloy And Mg-9Al-1Zn alloy AZ91D alloy	By the elimination of casting defects such as porosity and micro-segregation Charit and Mishra [68] has observed the grain size modified to approximately 0.68 µm whereas Chang et al. [69] has observed the grain size approximately to 85nm. The improvement in microhardness, fatigue property and ductility has been observed by applying number of passes and high strain rates at optimum parameters. Whereas another strange observation by Charit and Mishra [68] was that instability of microstructures and abnormal grain growth in processed region at temperature above 390°C but hardly any change in super-plasticity has been observed. Also, different parameters of material like grain boundary structure, grain size, dislocation density, etc. can be controlled by the nano-crystallization of the material via FSP.
Zahmatkesh et al. [71]	Hot rolled Plates of Al2024.	Higher Wear Resistance, Low value of coefficient of friction and improvement in micro-hardness in the nugget region have

		been the observations that Zahmatkesh et al. [71] has made due to modifications of grains to fine-equiaxed and of approximate size of 4µm after FSP. With increasing sliding distances increase in wear loss or weight loss of material has been observed but for FSP material, the curve has shown stable rate.
Balamurugan et al. [76]	AZ31B Magnesium Alloy	A comparison of two tool profiles was made in this study. The first tool profile was the Concave Shoulder Tool, and the second one was Step Shoulder Tool for Friction Stir Processing technique. A change in Strain Hardening effects, less wear rate and less wear loss, were observed with the concave shoulder tool; whereas in the case of the step shoulder tool, a significant role was played by grain size; and a higher value of wear loss and corrosion rates were observed.

2.2. Research Gap

The literature study depicts a few following gaps in the studies about magnesium alloys:

- There are a limited number of studies about the wear characteristics of friction stir processed magnesium-silicon based alloys. Earlier, more emphasis was given to the research of aluminium-based alloys and their mechanical and wear characteristics.
- The literature study suggests that most work has been done on studying the morphology and fine grain structures obtained after applying the friction stir processing technique. However, limited research is done showing the

improvement in mechanical and wear characteristics under high-temperature conditions.

2.3. Research Objectives

The following are the research objectives of the presented work:

- A comparative study of analysing the wear characteristics like the coefficient of friction and wear loss of Magnesium-Silicon alloy at high temperatures and under various loading conditions.
- The study of wear properties of as-cast AS21A alloy and Friction stir processed sample material at elevated temperatures.
- The study of specific wear rate for friction stir processed sample at high-temperature conditions and under various loadings.

Chapter-3

EXPERIMENTATION

This chapter has been organised in three sections. First section covers the preparation of the material for various tests. Second section covers the tests that were required to perform before the final wear test such as surfaces roughness test. Third section covers the objective of the thesis which was to perform the tribological test for the study of wear behaviour of the sample material.

3.1 Material Preparation:

Magnesium-Aluminium-Silicon based alloy (AS21A alloy) was prepared by the process of Gravity Die casting method and obtained from Venuka Engineering, Hyderabad, India. The dimensions of the casted material plate were 200×80×10 mm. The composition of the material was found to be Aluminium - 2.12%, Silicon –1.04%, Mn – 0.221%, Zn – 0.058%, Cu – 0.002%, Fe – 0.003%, Ni - <0.001%, Rest is Magnesium [72].

The material plate then made suitable for the process of Friction Stir Processing by machining the surface of the material plate. Friction Stir processing has been done on the material. The sample with 800rpm rotational speed was selected as optimum that has maximum value of surface micro-hardness that is 66 HV [72].

Friction Stir Welding Setup:

R V Machine Tools, FSW- 4T - HYD, is the setup for Friction Stir Process. This setup (as shown in Fig:3.1) is mainly use to perform the friction stir welding process and as we have already established that Friction Stir Processing is based on Friction Stir Welding therefore the setup of the same will be required to perform the experiment.

Table: 3.1 Specifications of the Friction Stir Welding setup:

Power	11KW
RPM of Spindle	Up to 3000rpm
Load Capacity	25kN
Clamps	Hydraulically actuated

There are two main purposes of the machine setup, first and foremost one is to generate heat due to friction and secondly to process this heat within the material sample. Therefore, it is tool that plays an important part in performing the action of heat generation, well designed and right tool profile has to be selected for the same. The tool has to penetrate in to the material and then has to perform the stirring operation in the material and also has to move along its length in order to perform stirring in the whole material. Table: 3.2 shows the specifications of the tool utilised for the process of Friction Stir Processing.

Table: 3.2 The specifications of the tool for the process of Friction Stir Processing.

Diameter of the shoulder	16mm, 20mm and 24mm
Tool material and its Hardness	H-13 Tool Steel and Hardness- 55HRC
Profile of Pin	Threaded Cylindrical with pitch of 1mm
Length of Probe	5mm
Diameter of Probe	6mm

Rotational Speed, Travel Speed and Shoulder Diameter are the most important parameters of the Friction Stir Processing. Therefore, optimised values of these parameters are calculated and then only the process can be successful in order to obtain desired characteristics in the material.

Three rotational speeds were 400rpm, 800rpm and 1200rpm selected for the process. The travel speeds of the tool were 20, 50 and 80mm/min selected while performing the process. The diameters of the shoulder were 16, 20 and 24mm. These were the input parameters for the process and were employed during the friction stir processing and allows the material to have desired properties in the stir zone of the material.

Thereafter, pins of cylindrical shapes of diameter 8 mm were cut from the processed area of the metal plate of AS21A alloy with the help of CNC wire cut machine. Similarly, samples of the pin were cut from as casted As21A plate for different characterisation tests.

The square plate of material SAE 304 SS was used for the bottom specimen of the wear machine. Fig: 3.1. shows the square plates and pins that are ready for wear test.

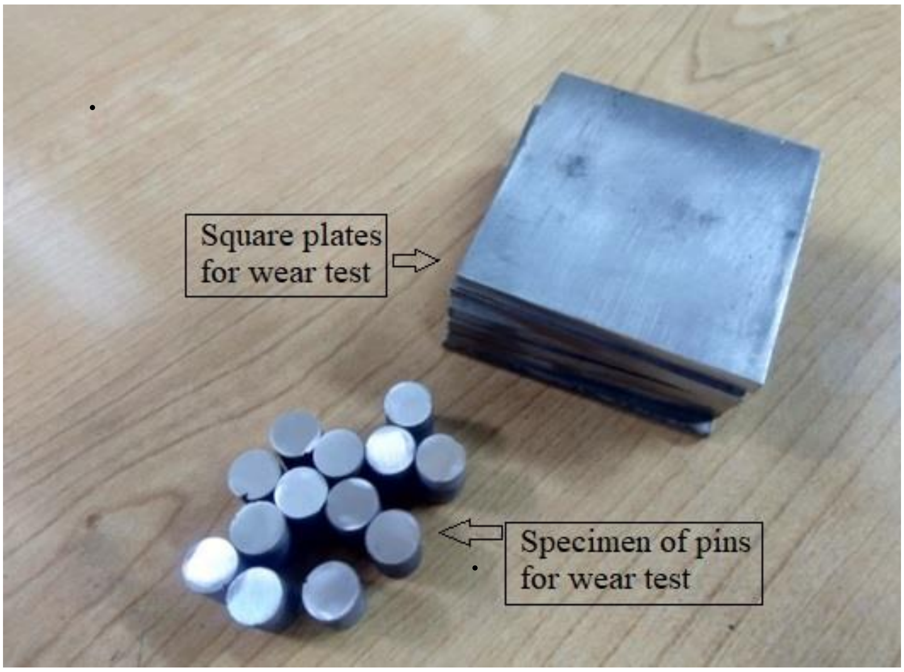

Fig: 3.1 Sample pins and Counter square plates for the Wear test

Hardness Test is utilised for the analysis of the micro-hardness of the sample materials. Fig: 3.2 shows an image of microhardness tester. Working principle of Microhardness tester involves an indenter of square pyramid shape with a 136^{o} angle between opposite faces and with an applied load of range 1kg to 120kg.

In this test a definite load is applied to the sample surface using the above briefed indenter for a duration of time. The area covered by the indenter was measured after the removal of load in terms of diagonal sides of the indenter.

The value of the hardness was obtained by the relation between area marked by the indenter and the load applied for that indentation. The following expression was used for the calculation of Vickers Hardness and indicated in terms of HV:

$$HV = \frac{1.8854\,P}{D^2} \qquad \ldots(3.1)$$

Here, P denotes the load applied during the test in kilograms

And D denotes diagonal length of the marked indentation on the sample surface in millimetres.

Fig: 3.2 Micro-hardness Tester

Samples were cleaned and polished before performing microhardness test, in order to remove any oxide layers or any other scales if present. The value of the hardness obtained was 55HV for the casted AS21A alloy material sample and it was 66HV for the Friction Stir Processed AS21A alloy material.

3.2 Surface Roughness Test

Surface roughness test was performed by using Taylor Hobson Surtronic 3+ as shown in Fig: 3.3. It is a portable type device that is used to measure the surface texture for calculating the surface roughness of the material sample and this device can be used in both laboratory as well as in the workshop.

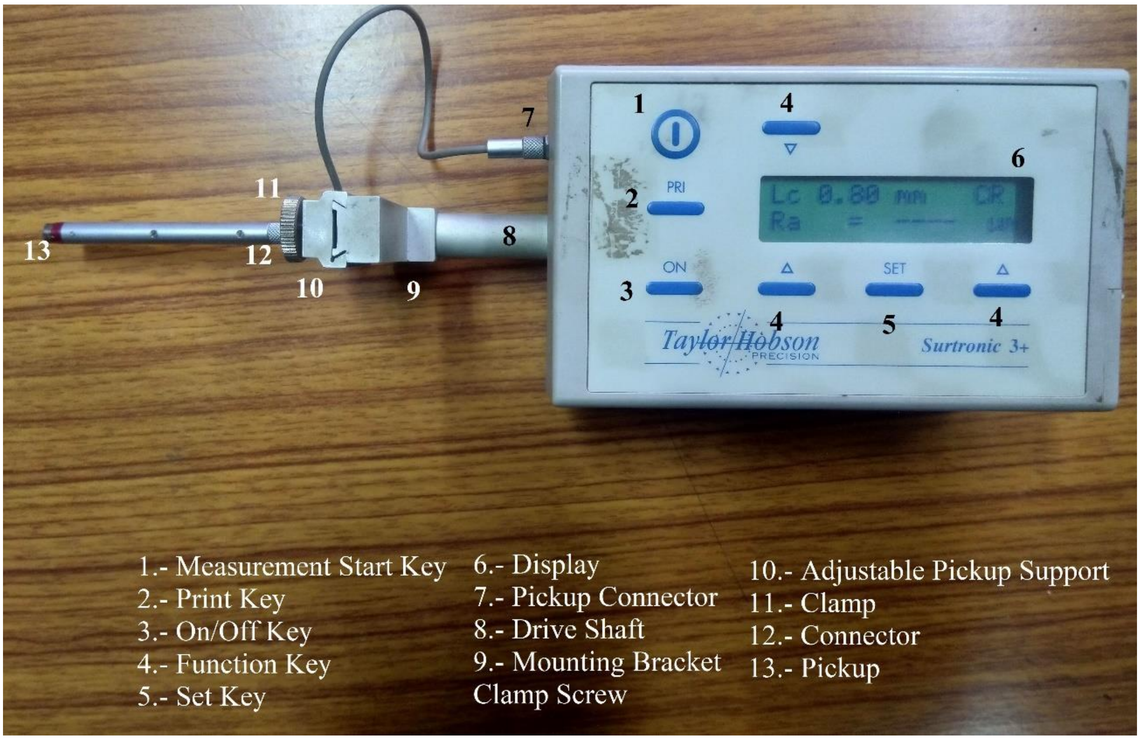

Fig: 3.3 Taylor Hobson Surface Roughness Tester

The device follows simple steps to perform surface roughness test.

Step one is to clean the surface with a clean cloth, preferably a microfiber cloth, so that if any dust particles present can be removed.

In step two, make sure the surface on which the sample material is placed is flat. We have used surface plate to place the samples as surface plate ensures the degree of flatness of the sample.

Then gently place the pickup of the tester on the surface that is to be measured. Keep sure that the pointer in the pickup is touching the surface.

Step three, press the measurement start key (The on/off key was already pressed before step one) and let the tester perform the test. The tester shows the reading in display as the value of Ra in micrometres (µm). Fig: 3.4 shows an example of machine testing a surface roughness.

The calibration of the machine can be done with help of ideal samples of specified surface roughness values, if the machine shows the same values, then we can be assured that the machine is working properly, otherwise a calibration process will be performed with the help of different function keys specified on the machine.

The roughness test performed for both of the material were performed and the values were taken two times and then the average of the two values were considered to be the final value for the surface roughness. The values for the sample pins and plates are given in Table 3.3.

Table:3.3 Values of Surface Roughness for pins and plate

	Sr. No.	Surface Roughness		Sr. No.	Surface Roughness
Specimen Pins	1	0.35	Square Plates	1	0.32
	2	0.38		2	0.39
	3	0.39		3	0.34
	4	0.36		4	0.35
	5	0.30		5	0.42
	6	0.28		6	0.30
	7	0.32		7	0.40
	8	0.36		8	0.28
	9	0.43		9	0.32
	10	0.31		10	0.38
	11	0.44		11	0.40
	12	0.30		12	0.38

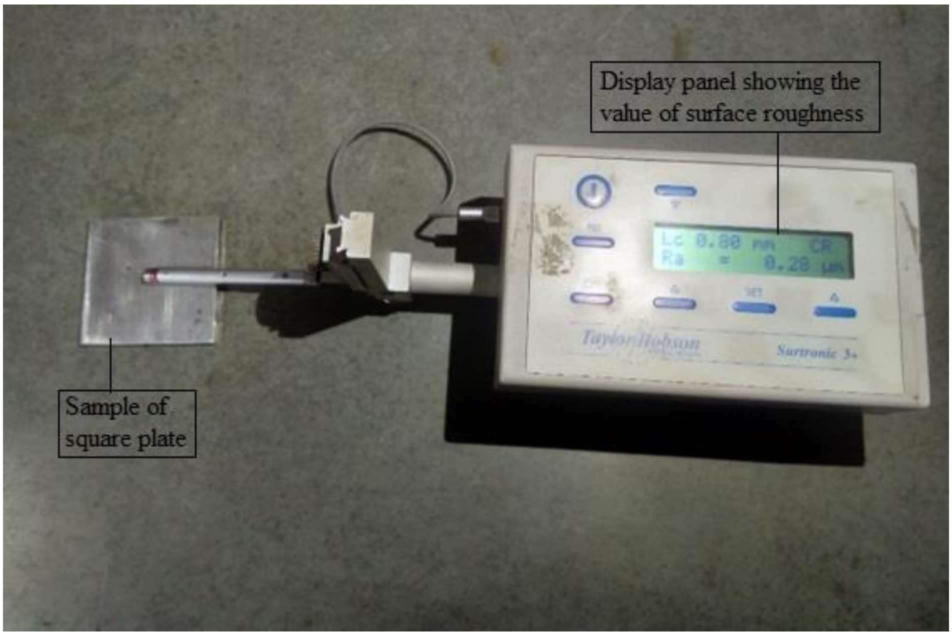

Fig: 3.4 Surface roughness tester with a sample

3.3 Wear Test:

Wear test or tribological test was performed to understand the wear behaviour of the material (Magnesium-Silicon alloy). The wear test was performed under dry conditions, meaning no lubricant was applied while performing the wear test and dry sliding of the sample material with the counter plate was performed.

Wear test was performed on the Linear Reciprocating Tribometer manufactured by Ducom Instruments. The test rig was shown in Fig: 3.5 and 3.6; and was capable of performing experiments in a wide range of temperature values from ambient to 550^{o}C.

The test rig consists of mainly two parts for testing, one that will be in rest position, no motion will be there in this section of the test rig. Other will have linear reciprocating motion, like in the case of present research, rest position was applied to the counter square plate and the linear reciprocating motion to the sample material pins.

Thereby, pins had made an impact on the square plate. The plates being hard material were not affected but pins being soft had some material loss or wear.

Fig: 3.5 Tribometer used for wear test

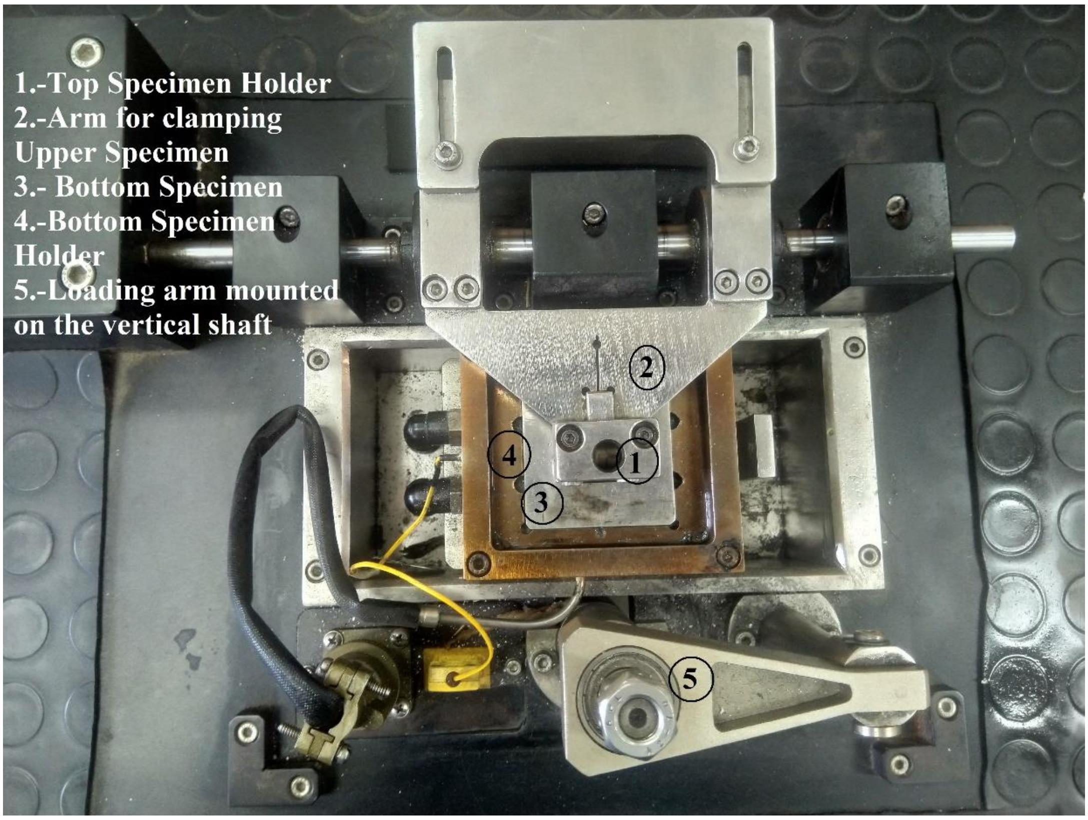

Fig: 3.6 Description of the environment chamber of tribometer

Table-3.4 Technical Specifications of the Tribometer:

Top Specimen	Spherical Ball of diameter range from 4mm to 12mm Cylindrical Pin of diameter range from 4mm to 12mm with a height maximum of 15mm
Bottom Specimen	Flat Plate of 50×50×5 mm
Normal Load	Dead weights in steps of 5N with a range from 5N to 50N
Frequency	Maximum value of 50Hz
Stroke Length	Ranges from 1mm to 20mm in the following manner **Frequency (in Hz)** **Stroke Length (in mm)** 1 – 8 20 8 – 10 16 10 – 20 15 20 – 30 5 30 – 40 2 40 – 50 1

Frictional Force	Ranges from 0 to 50N
Temperature	Ranges from ambient to 550°C

The wear test was conducted in different temperature ranges and before performing the test, samples were rubbed against 800-1200 grit emery paper so that proper observations can be obtained. The different parameters like load, temperature, frequency, stroke length, etc. of the Linear reciprocating tribometer were shown in Table-3.4.

The rate of specific wear is calculated by the following relation:

$$Specific\ Wear\ Rate = \frac{Volume\ loss\ in\ cubic\ millimeter}{Normal\ Load\ (in\ N) \times Sliding\ distance\ (in\ mm)} \quad ...(3.2)$$

The volume loss can be calculated by the ratio of weight loss (in grams) to the density (in g/cm^3) of the samples. The weight loss can also be calculated by weighing the samples after and before the test.

These samples were rinsed in acetone solution every time, to measure the weight. Electronic apparatus was used for measuring the weight and the apparatus was having an accuracy of 0.001mg.

Coefficient of friction can be measured with the help of sensors connected to the linear reciprocating tribometer test rig. The value of Coefficient of Friction between the sample and the plate is the ratio between frictional force and the normal load. The value of frictional force can be obtained from the tribometer and the value of normal load is the known value of dead weights applied manually.

The expression for the Coefficient of Friction is:

$$Cofficient\ of\ Friction = \frac{Friction\ Force\ (in\ N)}{Normal\ Load\ (in\ N)} \quad ...(3.3)$$

Table 3.5 describes the parameters that will be performed on the tribometer. The specifications of the pins (Friction stir processed sample material) and the specifications of the plate against which the pins will be rubbed are given in Table:3.5.

Table:3.5 Parameters for the wear test

Parameters	**Value**
Normal Load	10N, 20N and 30N
Stroke Length	10mm
Frequency	10Hz
Temperature	50^{o}C, 100^{o}C, 150^{o}C and 200^{o}C
Operating Time	600 seconds
Diameter of Pin	8mm
Ra value of Pin	**0.28μm to 0.44μm**
Bottom Plate	SAE 304 SS (42 HRC)
Bottom Plate Size	50 × 50 × 5 mm
Ra Value of Bottom Plate	0.28μm to 0.40μm

Chapter-4

RESULTS AND DISCUSSION

Friction Sir Processing has eliminated the different casting defects which were present in the casted AS21A material and the resulted material has better mechanical characteristics after the operation.

- The Ultimate Tensile Strength in MPa has improved to 88.6 MPa from 83.2 MPa.
- The change in Percentage Elongation was observed from 3.87 to 10.6.
- The value of Microhardness of processed material was noticed as 66 HV as earlier it was 55 HV in casted material.

The observations have shown that defects present in the base material of AS21A were removed. The coarse grain structure of material particles was altered and modified to a fine grain structure that leads to improved mechanical properties; mainly, ductility has shown more remarkable improvement.

The microstructural changes in the material were represented by SEM images of the sample. Fig:4.1 shows the different samples before and after the friction stir processing of the sample. Fig:4.1(a) depicted that the as-cast sample of AS21A alloy consisted of intermetallic coarse grain structure, and the representation of Chinese script was observed. The coarse grain structure of the sample was modified after the friction stir processing technique as it has improved its structure to refined grains [72], as shown in Fig:4.1(b).

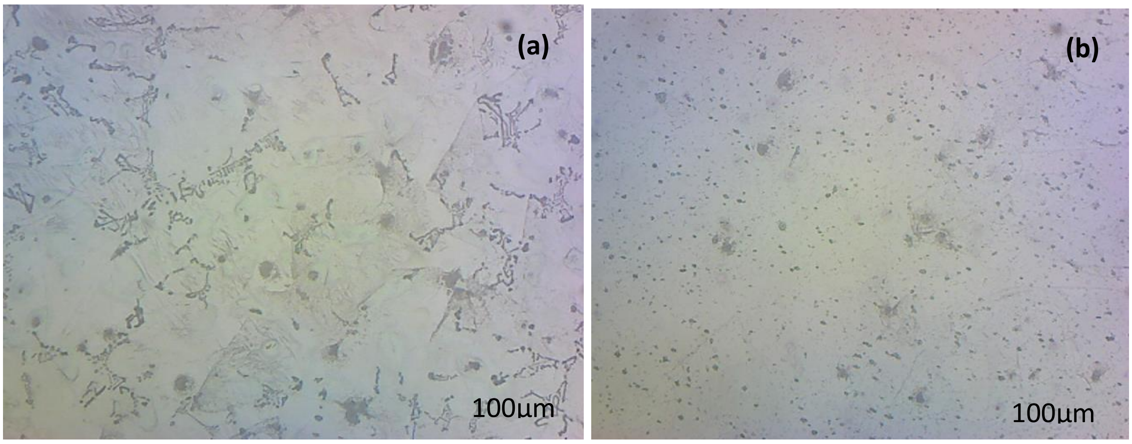

Fig: 4.1 SEM image of AS21A alloy (a) as-cast AS21A alloy (b) Friction Stir Processed AS21A alloy

The percentage elongation obtained after the operation was about 11% and achieved at 800 rpm of rotational tool speed. In contrast, the profile of the tool pin was cylindrically threaded during friction stir processing.

The wear characteristics of Friction Stir Processed AS21A alloy were characterised on Linear Reciprocating Tribometer. The obtained value of frictional forces and coefficient of friction at different temperatures were formulated in a table (Table 4.1) as shown below:

Table 4.1 Coefficient of Friction for AS21A alloy of Friction Stir Processed samples for different loads at different temperatures

Load (in N)	Temperature (in ^{o}C)	Friction Force (in N)	Coefficient of Friction
10	50	3.75	**0.37**
	100	3.97	**0.39**
	150	4.13	**0.41**
	200	4.45	**0.44**
20	50	5.23	**0.26**
	100	5.53	**0.28**
	150	6.13	**0.31**
	200	6.54	**0.33**
30	50	6.89	**0.23**
	100	7.53	**0.25**
	150	8.59	**0.29**
	200	9.28	**0.31**

The data from Table 4.1 has shown an increment in the value of the coefficient of friction as the temperature rises for a specified value of the load. However, if we look closely at the values, two significant things can be observed. First, there was a gradual change in the values, and second, there was some considerable change as we increased the temperature.

For 10N load, an increment of about 5% to 7% in the values was observed as we increased the temperature from 50^{o}C to 200^{o}C. Likewise, moving to 20N load and 30N load, the changes were increased from about 6% to 10%, and about 6% to 16%, respectively.

Moreover, if we look at this data from another perspective, we can see that with the increase in load by keeping the temperature constant, a drop in the value was noted, and it was about 24% to 29% while moving from 10N to 20N and about 6% to 11% while moving from 20N to 30N.

It was noted because of the inverse relation of applied load with the coefficient of friction as detailed in equation 3.3 of the previous chapter. Therefore, there was a reduction in the coefficient of friction. However, the other thing to note is that there was a drastic change when the load was first increased from 10N to 20N compared to when it increased from 20N to 30N.

The primary reason for this behaviour was the formation of metal oxides that usually form during metal-metal sliding, leading to a decrease in friction [73]. Further, it was noted in Fig: 4.2 that as temperature increased, the smoothness of the curve was also affected significantly. Fig:4.2 (a) and (b) have shown variations for 50^{o}C and 100^{o}C, respectively, for 10N, 20N, and 30N of coefficient of friction with time. There were no considerable variations in the graph, and values moved within a limit and were not change drastically. From Fig 4.2 (c) and (d), significant variations in the values were observed with respect to time and have shown some sudden increments as the temperature was increased from 100^{o}C to 150^{o}C and 200^{o}C. The primary reason for the same was of increase in temperature.

The reason for the same was an increase in temperature. As temperature increases, it leads to an increase in wear and adhesion [74]. That increases the roughness of the material surface, and an increase in the value of the coefficient of friction was noticed and wear debris was also present in between, which can lead to sudden changes in the values as shown in the graph.

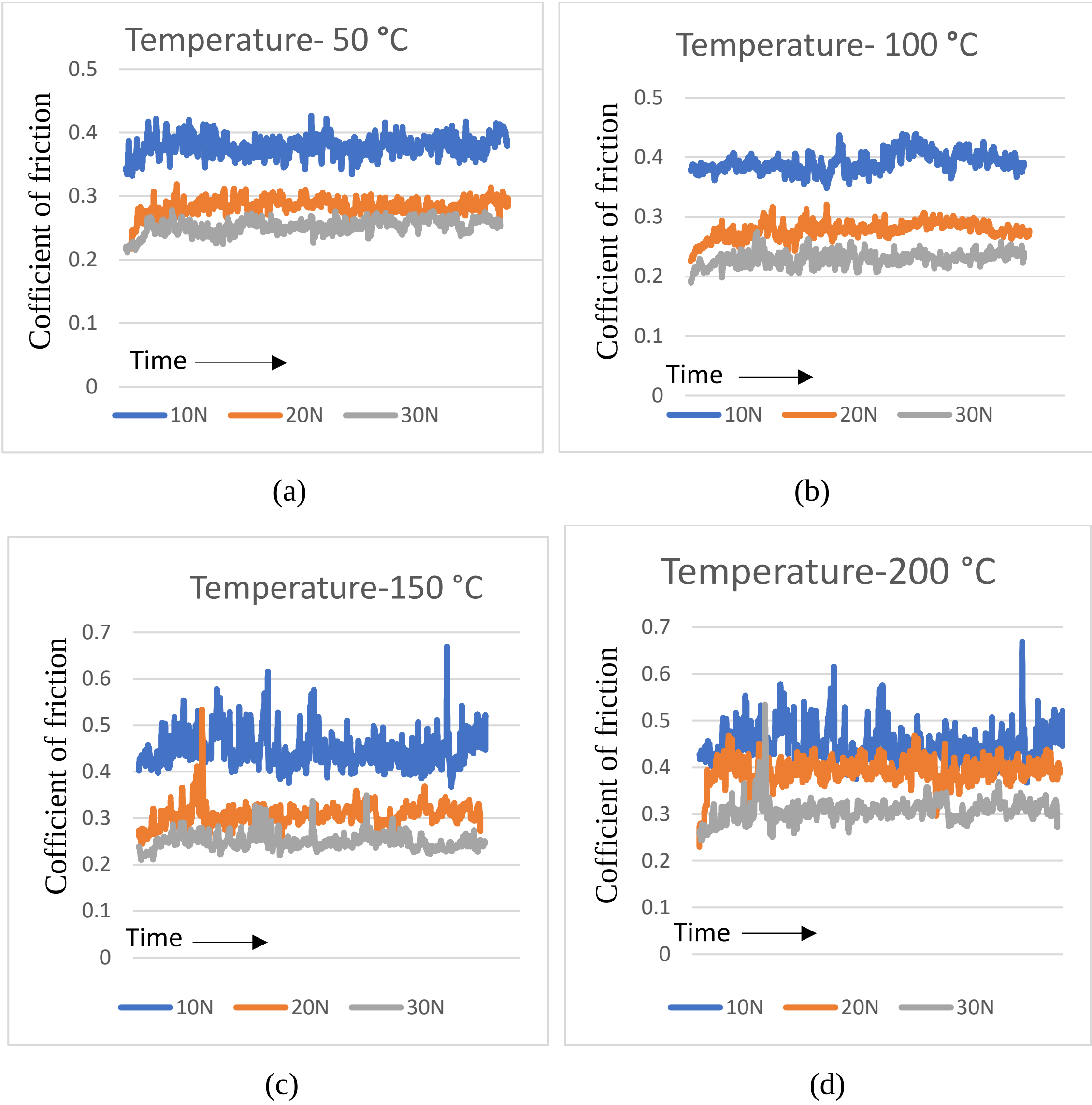

Fig: 4.2 Variation of Coefficient of Friction with time for different loads at 50°C, 100°C, 150°C and 200°C

Fig: 4.3, 4.4 and 4.5 represented the variation in the coefficient of friction with time, keeping the load constant, and we can see from the figures that for any particular load, more variations were observed in the case of high temperature.

Apart from that, a gradual increase in the average values and variation in values of the coefficient of friction was also observed. As the temperature of the surfaces increases, the asperities present on the interface also increases. These high asperities present on the surface now led to the hindrances during sliding, and sudden drop and increase in the value of frictional force were observed [74]. That led to the increased waviness in the graph of the coefficient of friction with time for elevated temperatures.

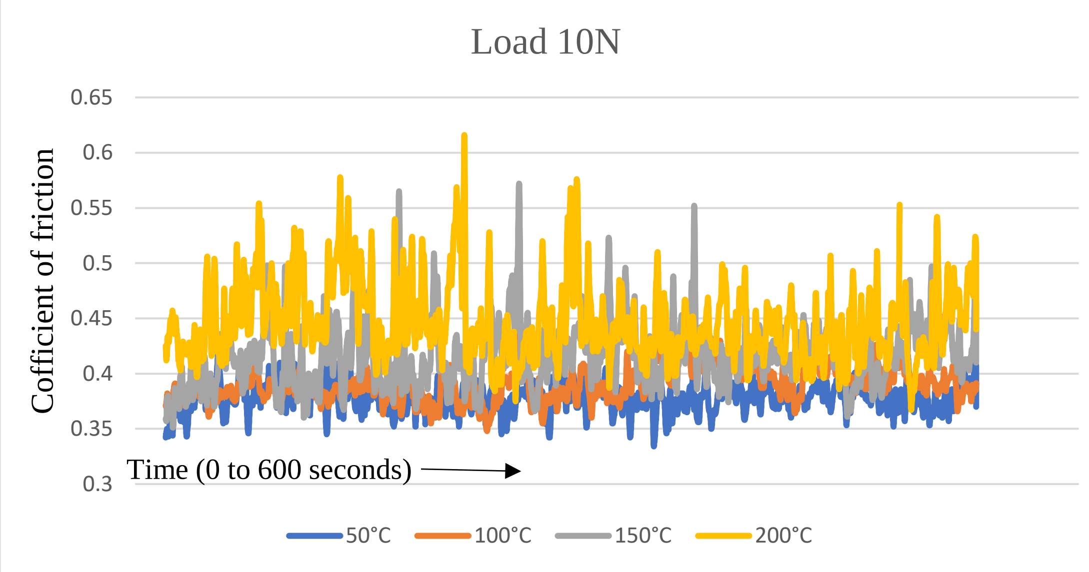

Fig: 4.3 Variation of Coefficient of Friction with time for different temperatures at a load of 10N

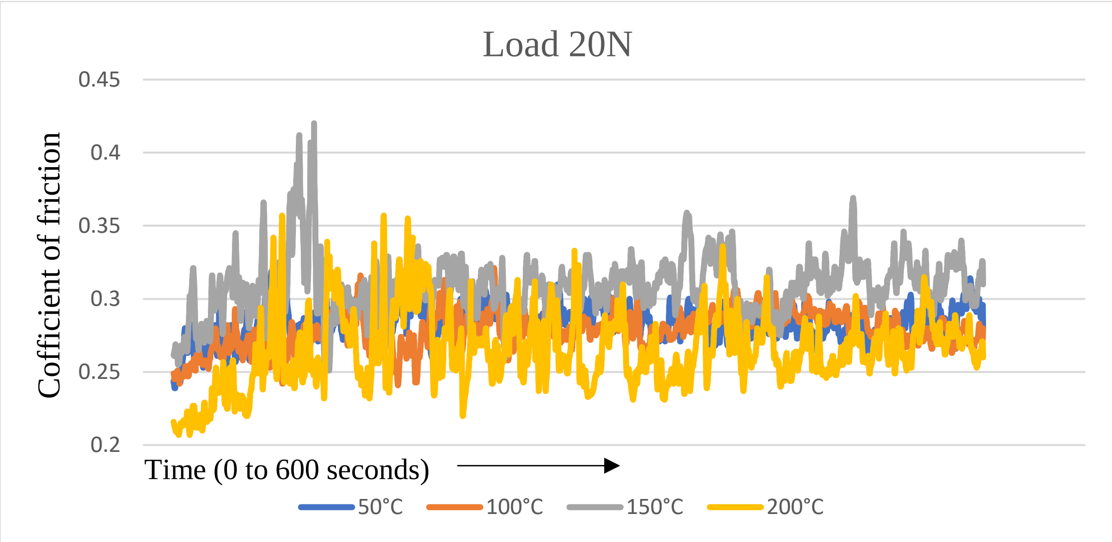

Fig: 4.4 Variation of Coefficient of Friction with time for different temperatures at a load of 20N

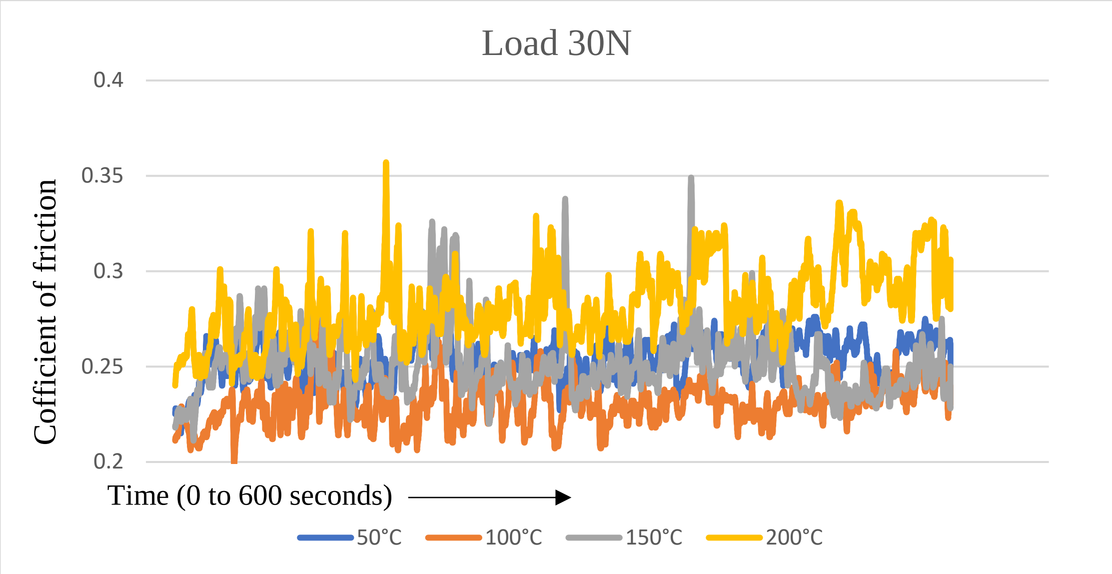

Fig: 4.5 Variation of Coefficient of Friction with time for different temperatures at a load of 30N

The following table 4.2 shows the variation in the wear loss of the sample with changes in temperature and changes in loading conditions. The wear loss of the samples was calculated by carefully weighing them before and after every test process in the electronic weighing balance.

Table 4.2 Change in weight of the samples after the test with different loads and at different temperatures

Load (in N)	Temperature (in ^{o}C)	Change in Weight (in mg)
10	50	44
	100	32
	150	26
	200	24
20	50	44
	100	40
	150	39
	200	36
30	50	47
	100	38
	150	35
	200	35

Graphs from Fig: 4.6 shows that with the increase in load for a specific temperature, there was an increase in the value of wear loss. From Fig: 4.6 (a), for 50°C, while increasing load to 20N, wear loss was observed to be identical, but when the load was increased to 30N, an increase in the wear loss was noted. Likewise, observations from Fig: 4.6 (b), for 100°C, an increase in the value of wear loss was present as we increased the load but here, it decreased again for the load of 30N. A similar increase and decrease were observed in Fig: 4.6 (c) and (d) for temperatures 150°C and 200°C, respectively.

The increase in wear loss due to an increase in load was noted because as the load increases, the removal of material from the surface of the pins was increased due to surface erosion phenomena of plastic deformation and delamination of the layers of material surface [75].

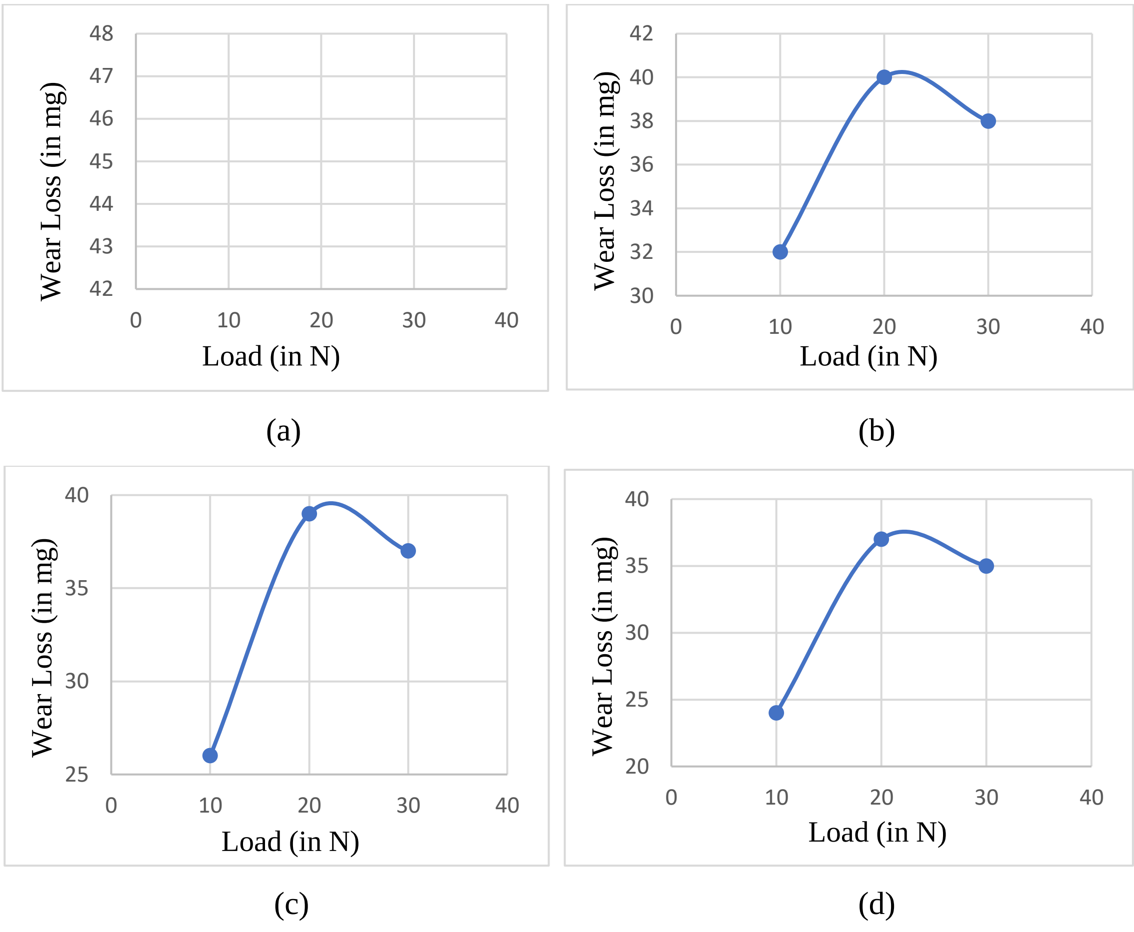

Fig: 4.6 Graph wear loss versus load at different temperatures

Fig:4.7 shows the variation of wear loss with the temperature at constant load value as Fig:4.7(a) shows the variation for 10N load, Fig:4.7(b) for 20N load, and Fig:4.7(c) for 30N load; and all the values for wear loss are for different temperatures like 50°C, 100°C, 150°C and 200°C. The variations in Fig:4.7 suggested that with the increase in temperature value, there was a decrease in the volume of material removal from the surface of the specimen by keeping the load constant.

On the other hand, at low temperatures like ambient or 50^{o}C, the surface showed properties like the low value of hardness and high ductility value that allowed the sliding motion to have a significant value of wear or material removal. However, if the temperature increases, it leads to the formation of some hard phases of Mg_2Si on the surface of the AS21A alloy. These hard phases allowed the material to have greater hardness, which slowed the material removal from the surface [75].

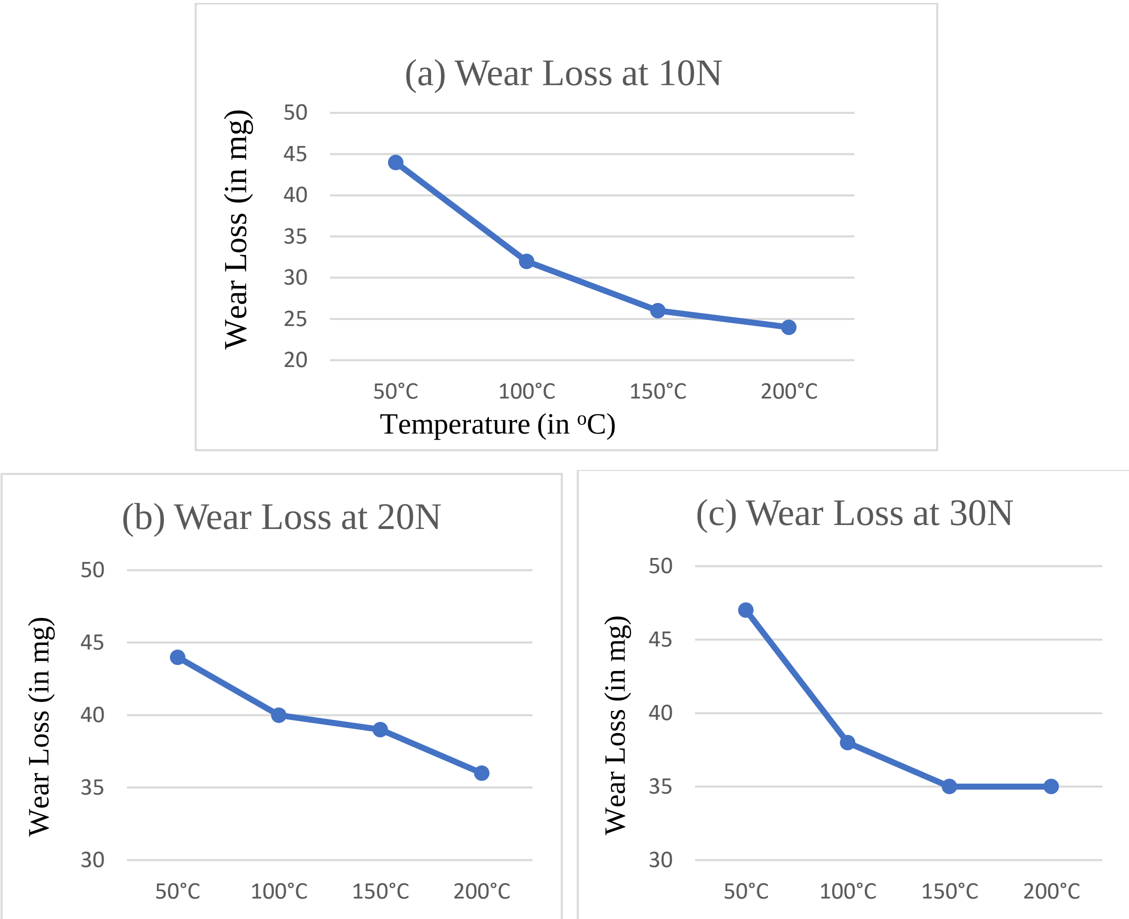

Fig: 4.7 Graphs showing plots of wear loss versus temperatures for different loads (a) 10N, (b) 20N, (c) 30N

Also, the comparison of samples of as-cast AS21A alloy and Friction Stir Processed AS21A alloy was made and shown in Table 4.3 and Table 4.4. Table 4.3 compares the values of the coefficient of friction with different loads and for different values of temperatures. Table 4.4 compares the value of wear loss with load and for different temperatures.

Table 4.3 Comparison of the values of coefficient of friction of the processed and as-cast AS21A alloy at different temperature conditions

Load	As-Cast AS21A alloy	FSPed AS21A alloy in ambient conditions	FSPed AS21A alloy at 50°C	FSPed AS21A alloy at 100°C	FSPed AS21A alloy at 150°C	FSPed AS21A alloy at 200°C
10	0.32	0.31	0.37	0.39	0.41	0.44
20	0.29	0.26	0.26	0.28	0.31	0.33
30	0.24	0.23	0.23	0.25	0.29	0.31

Table 4.4 Comparison of the values of wear loss of the processed and as-cast AS21A alloy at different temperature conditions

Load	As-Cast AS21A alloy	FSPed AS21A alloy in ambient conditions	FSPed AS21A alloy at 50°C	FSPed AS21A alloy at 100°C	FSPed AS21A alloy at 150°C	FSPed AS21A alloy at 200°C
10	34.2	26.2	44	32	26	24
20	49.2	40.9	44	40	39	36
30	60	57.2	47	38	35	35

Comparing the samples as-cast and Friction Stir Processed based on the coefficient of friction in Fig:4.9. It can be observed that the minimum value was in ambient conditions, and there was a slight increment in the as-cast sample as compared to ambient conditions. Then, with the increase in temperature, there was a continuous increment due to the material's surface properties.

Another comparison was made based on the wear loss of the samples of as-cast AS21A alloy and Friction Stir Processed AS21A alloy with loading conditions and at different temperatures in Fig:4.8. The graph, shown in Fig:4.10, clearly depicted that Friction Stir Processed sample has better wear characteristics as there was a decrease in volume loss during the sliding motion.

Moreover, graphs explained that even at ambient conditions, AS21A alloys show better wear properties than the as-cast sample and improved as temperature increased for the testing.

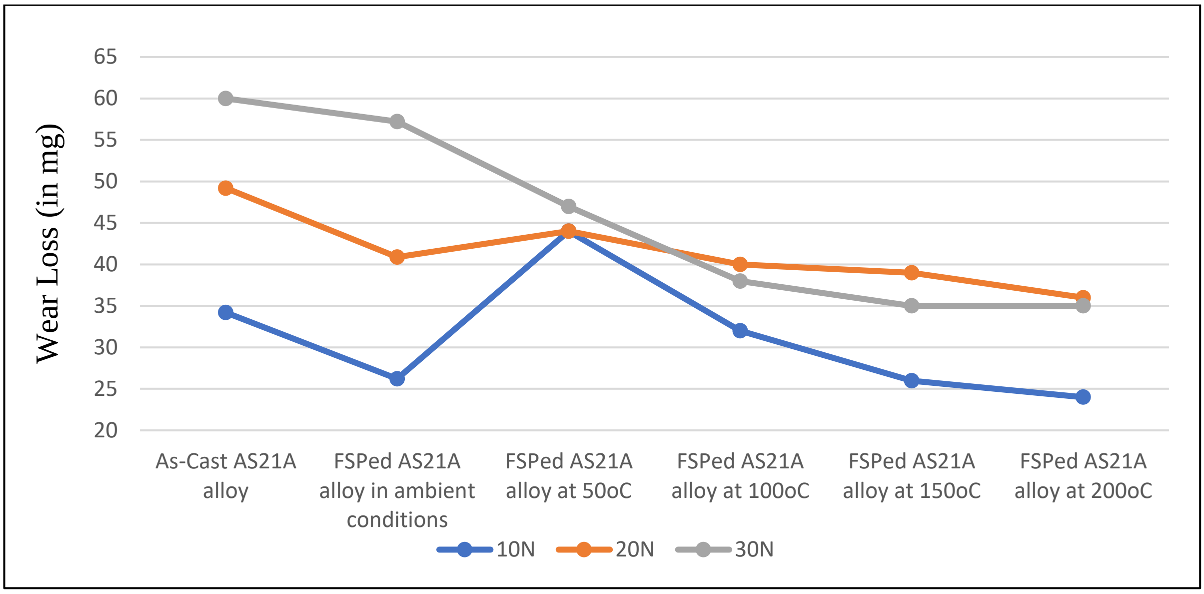

Fig 4.8 Graphical representation of Wear Loss at different load and temperature conditions

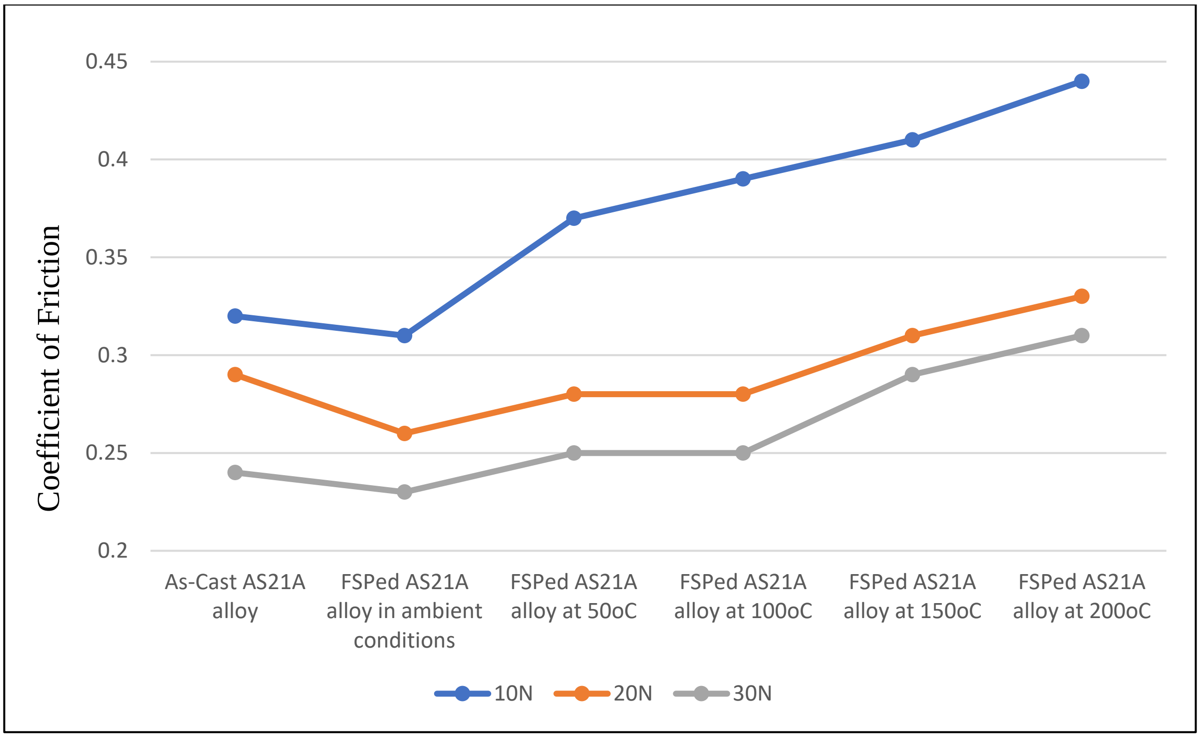

Fig 4.9 Graphical representation of Coefficient of Friction at different load and temperature conditions

The value of the specific wear rate was calculated using equation 3.2, and the values were presented in Table:4.5. From the table, it could be noted that as the value of temperature increases, there was a decrease in the value of specific wear rate. Similarly, there was a decrease in the value of specific wear rate for increased load for a particular temperature. Likewise, the observations shown in Fig:4.10 explained a decrease in the value of specific wear rates either there was an increase in temperature or load, which indicated improvement in wear properties at higher values of loads [77].

Table: 4.5 The values of specific wear rate (in 10^{-8} mm^3/Nm) for different temperature values and load values

Temperature (°C) Load (in N)	50°C	100°C	150°C	200°C
10	2.16	1.27	1.27	1.17
20	2.16	0.98	0.96	0.88
30	0.77	0.62	0.57	0.57

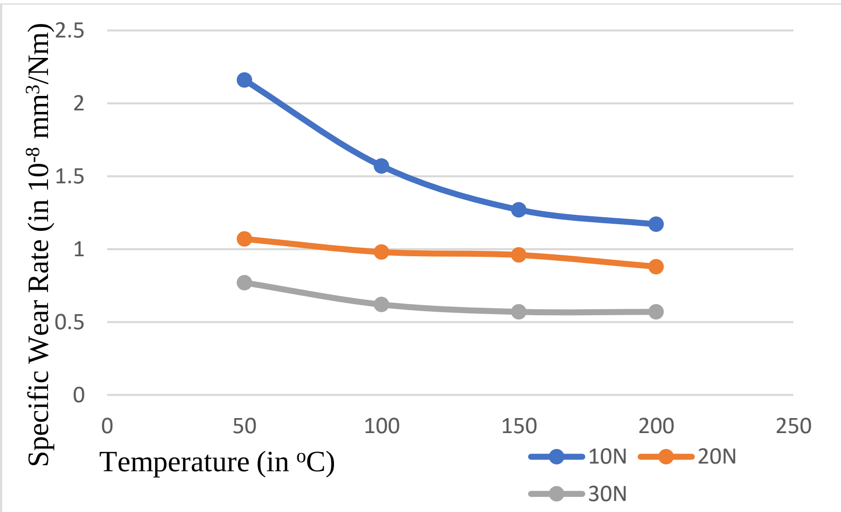

Fig:4.10 Variation of specific wear rate with respect to load and temperature

The values of specific wear rates range from 10^{-4} to 10^{-8} (mm^3/Nm) fall under the category of mild wear and defined as a small value of wear that occurred due to oxidative wear [78]. The present case was of the same order. Therefore, wear for magnesium silicon

AS21A alloy for the current linear reciprocating tribometer test was categorised as mild wear. Most studies on specific wear rates were for different sliding velocities rather than different temperatures. The different values of sliding velocities have changed the type of wear mechanism for the material tested [79]. Moreover, with the increase in temperature, oxidation of the surface layer starts, which affects the surface characteristics. If a further rise in temperature was noted, it caused microstructural changes in the material. [80] That changes the whole wear mechanisms for the sample material.

Chapter-5

CONCLUSIONS AND FUTURE SCOPE

5.1. Conclusions

The parent material selected for the current study was Magnesium-Silicon based alloy. Magnesium-Silicon based aluminium alloy is a kind of heat-resistant material. A Friction Stir Processed AS21A alloy was tested for wear characteristics in work presented here. The effects of temperatures and normal loads were analysed while sliding AS21A alloy pins were rubbed against a hard steel plate. Different changes were observed that are better than as-cast AS21A alloy. The primary reason for the changes or improvements in the samples was the homogeneous mixture of particles after the friction stir processing of the samples. Friction stir processing allowed the parent material to have better mechanical and wear characteristics [72].

The following conclusions were made based on testing the friction stir processed samples on the Linear Reciprocating Tribometer. Overall, an improvement in the samples was observed and proved that Magnesium-silicon-based alloys are a worthy material for heat-resistant applications.

(1) For a specific temperature value, the value of the coefficient of friction decreases about 6% to 29% with the increase in loading conditions. Whereas, for one particular value of the load, the value of the coefficient of friction increases about 5% to 16% with the temperature rise.

(2) On the other hand, wear loss has shown different behaviour. By keeping the value of temperature constant and by increasing the value of the load, there was first an increase in the value of wear loss then some reduction was also observed. Unlike

this, with the increase in temperature for a particular load, the value of wear loss decreases gradually, showing better wear properties at elevated temperatures.

(3) The value of the specific wear rate (in terms of 10^{-4} mm^3/Nm) changes from 2.16 to 0.77, 1.57 to 0.62, 1.27 to 0.57 and 1.17 to 0.57 for different temperatures of 50^{o}C, 100^{o}C, 150^{o}C and 200^{o}C respectively. That shows that Magnesium alloys show good wear characteristics in high-temperature values.

(4) On comparing the friction stir processed sample with the as-cast sample, there was only a slight change noticed in the value of the coefficient of friction as we increased the value of the load. But there was a decrease in the values. However, as the temperature increased, there was a significant change in the processed sample.

(5) Wear loss of as-cast AS21A alloy when compared with processed AS21A alloy samples, a considerable improvement was observed. There was an increase in wear loss in both the samples as we increased load, but in the processed sample, the value decreased compared to the as-cast sample. That was the primary reason for performing the friction stir processing so that wear loss could be reduced.

(6) The wear properties of the AS21A alloy have been improved with the help of the friction stir processing technique as wear loss reduces with the increase in temperature conditions, compared to the wear loss of the ambient conditions. A drastic increase in wear loss was observed in ambient conditions, whereas there was only a slight increase in the wear loss for elevated temperatures.

(7) AS21A alloy has shown better characteristics in high-temperature conditions because of the friction stir processing. This technique allowed the particles of the alloys to be mixed homogeneously and made a fine grain particle structure in the alloy that helped the samples to perform better. Even at high temperatures, the

surface forms a hard layer of the Mg_2Si phase, preventing the wear loss in the material, making it a heat-resistant property of the material.

5.2. Future Scope of the work

- The current work presents the wear behaviour of AS21A alloy for elevated temperature conditions as it was a heat-resistant material. Since there are more parameters to predict the wear behaviour, some of those parameters can be considered in future to assess the wear behaviour of the material.
- The wet sliding test can be conducted to explore more aspects of the wear characteristics of the sample material under ambient conditions and for high-temperature conditions as well.

REFERNCES

1. Musfirah, A. H., & Jaharah, A. G. (2012). Magnesium and aluminum alloys in automotive industry. J. Appl. Sci. Res, 8(9), 4865-4875.
2. Pervaiz, M., Panthapulakkal, S., Sain, M., & Tjong, J. (2016). Emerging trends in automotive lightweighting through novel composite materials. Materials Sciences and Applications, 7(01), 26.
3. Čížek, L., Greger, M., Pawlica, L., Dobrzański, L. A., & Tański, T. (2004). Study of selected properties of magnesium alloy AZ91 after heat treatment and forming. Journal of Materials Processing Technology, 157, 466-471.
4. Mordike, B. L., & Ebert, T. (2001). Magnesium: properties—applications—potential. Materials Science and Engineering: A, 302(1), 37-45.
5. Radha, R., & Sreekanth, D. (2017). Insight of magnesium alloys and composites for orthopedic implant applications–a review. Journal of magnesium and alloys, 5(3), 286-312.
6. Polmear, I., StJohn, D., Nie, J. F., & Qian, M. (2017). Light alloys: metallurgy of the light metals. Butterworth-Heinemann.
7. Ghali, E. (2010). Properties, Use, and Performance of Magnesium and Its Alloys. Winston Revie R., Corrosion Resistance of Aluminum and Magnesium Alloys: Understanding, Performance, and Testing.
8. Luo, A. A. (2004). Recent magnesium alloy development for elevated temperature applications. International materials reviews, 49(1), 13-30.
9. Candan, S., & Candan, E. (2017). A comparative study on corrosion of Mg–Al–Si alloys. Transactions of Nonferrous Metals Society of China, 27(8), 1725-1734.
10. Yang, W. G., & Koo, C. H. (2003). Tensile properties of Mg-8Al-xRE alloys from 300 K to 673 K. Materials Transactions, 44(5), 1029-1035.

11. Mabuchi, M., Kubota, K., & Higashi, K. (1996). Elevated temperature mechanical properties of magnesium alloys containing Mg2Si. Materials science and technology, 12(1), 35-39.
12. Stathokostopoulos, D., Chaliampalias, D., Stefanaki, E. C., Polymeris, G., Pavlidou, E., Chrissafis, K., Hatzikraniotis E., Paraskevopoulos K. M. & Vourlias, G. (2013). Structure, morphology and electrical properties of Mg2Si layers deposited by pack cementation. Applied surface science, 285, 417-424..
13. Ma, G. R., Li, X. L., Li, L., Wang, X., & Li, Q. F. (2011). Modification of Mg2Si morphology in Mg–9% Al–0.7% Si alloy by the SIMA process. Materials Characterization, 62(3), 360-366.
14. Gan, W. M., Wu, K., Zheng, M. Y., Wang, X. J., Chang, H., & Brokmeier, H. G. (2009). Microstructure and mechanical property of the ECAPed Mg2Si/Mg composite. Materials Science and Engineering: A, 516(1-2), 283-289.
15. Aly, M., Hashmi, M. S. J., Olabi, A. G., Messeiry, M., & Hussain, A. I. (2011). Effect of nano clay particles on mechanical, thermal and physical behaviours of waste-glass cement mortars. Materials Science and Engineering: A, 528(27), 7991-7998.
16. Wang, Q., Chen, Y., Liu, M., Lin, J., & Roven, H. J. (2010). Microstructure evolution of AZ series magnesium alloys during cyclic extrusion compression. Materials Science and Engineering: A, 527(9), 2265-2273.
17. Yan, X. U., Hu, L. X., Yu, S. U. N., Jia, J. B., & Jiang, J. F. (2015). Microstructure and mechanical properties of AZ61 magnesium alloy prepared by repetitive upsetting-extrusion. Transactions of Nonferrous Metals Society of China, 25(2), 381-388.
18. Guo, W., Wang, Q., Ye, B., & Zhou, H. (2013). Microstructure and mechanical properties of AZ31 magnesium alloy processed by cyclic closed-die forging. Journal of Alloys and Compounds, 558, 164-171.

19. Darras, B. M., Khraisheh, M. K., Abu-Farha, F. K., & Omar, M. A. (2007). Friction stir processing of commercial AZ31 magnesium alloy. Journal of materials processing technology, 191(1-3), 77-81.
20. Mishra, R. S., & Ma, Z. Y. (2005). Friction stir welding and processing. Materials science and engineering: R: reports, 50(1-2), 1-78.
21. Mironov, S., Sato, Y. S., & Kokawa, H. (2019). Friction-stir processing. In Nanocrystalline Titanium (pp. 55-69). Elsevier.
22. Nakata, K., Kim, Y. G., Fujii, H., Tsumura, T., & Komazaki, T. (2006). Improvement of mechanical properties of aluminum die casting alloy by multi-pass friction stir processing. Materials Science and Engineering: A, 437(2), 274-280.
23. Abbasi-Baharanchi, M., Karimzadeh, F., & Enayati, M. H. (2016). Effects of friction stir process parameters on microstructure and mechanical properties of aluminum powder metallurgy parts. Journal of Advanced Materials and Processing, 4(1), 38-55.
24. Izadi, H., Nolting, A., Munro, C., Bishop, D. P., Plucknett, K. P., & Gerlich, A. P. (2013). Friction stir processing of Al/SiC composites fabricated by powder metallurgy. Journal of Materials Processing Technology, 213(11), 1900-1907.
25. Jeon, C. H., Jeong, Y. H., Seo, J. J., Tien, H. N., Hong, S. T., Yum, Y. J., Hur, S. H., & Lee, K. J. (2014). Material properties of graphene/aluminum metal matrix composites fabricated by friction stir processing. International Journal of Precision Engineering and Manufacturing, 15(6), 1235-1239.
26. Sunil, B. R., Reddy, G. P. K., Patle, H., & Dumpala, R. (2016). Magnesium based surface metal matrix composites by friction stir processing. Journal of Magnesium and alloys, 4(1), 52-61.

27. Sharma, D. K., Badheka, V., Patel, V., & Upadhyay, G. (2021). Recent developments in hybrid surface metal matrix composites produced by friction stir processing: A review. Journal of Tribology, 143(5).
28. Grujicic, M., Arakere, G., Yalavarthy, H. V., He, T., Yen, C. F., & Cheeseman, B. A. (2010). Modeling of AA5083 material-microstructure evolution during butt friction-stir welding. Journal of Materials Engineering and Performance, 19(5), 672-684.
29. Ma, Z. Y. (2008). Friction stir processing technology: a review. Metallurgical and materials Transactions A, 39(3), 642-658.
30. Mahoney, M. W., Rhodes, C. G., Flintoff, J. G., Bingel, W. H., & Spurling, R. A. (1998). Properties of friction-stir-welded 7075 T651 aluminum. Metallurgical and materials transactions A, 29(7), 1955-1964.
31. Chang, C., Du, X. H., & Huang, J. C. (2008). Producing nanograined microstructure in Mg–Al–Zn alloy by two-step friction stir processing. Scripta materialia, 59(3), 356-359.
32. Azizieh, M., Kokabi, A. H., & Abachi, P. (2011). Effect of rotational speed and probe profile on microstructure and hardness of AZ31/Al2O3 nanocomposites fabricated by friction stir processing. Materials & Design, 32(4), 2034-2041.
33. Elangovan, K., & Balasubramanian, V. (2008). Influences of tool pin profile and welding speed on the formation of friction stir processing zone in AA2219 aluminium alloy. Journal of materials processing technology, 200(1-3), 163-175.
34. SUMIT, J. (2021). TRIBOLOGICAL BEHAVIOURS OF MAGNESIUM ALLOY SECTOR SHAPE PAD WITH SURFACE MODIFICATION (Doctoral dissertation).
35. Yadav, D., & Bauri, R. (2012). Effect of friction stir processing on microstructure and mechanical properties of aluminium. Materials Science and Engineering: A, 539, 85-92.

36. Nandan, R., Roy, G. G., & Debroy, T. (2006). Numerical simulation of three-dimensional heat transfer and plastic flow during friction stir welding. Metallurgical and materials transactions A, 37(4), 1247-1259.
37. Buckley, D. H. (1981). Surface effects in adhesion, friction, wear, and lubrication (Vol. 5). Elsevier.
38. Dwivedi, D. K. (2010). Adhesive wear behaviour of cast aluminium–silicon alloys: Overview. Materials & Design (1980-2015), 31(5), 2517-2531.
39. Deuis, R. L., Subramanian, C., & Yellup, J. M. (1996). Abrasive wear of aluminium composites—a review. wear, 201(1-2), 132-144.
40. Olugbade, T. O., Omiyale, B. O., & Ojo, O. T. (2021). Corrosion, corrosion fatigue, and protection of magnesium alloys: Mechanisms, measurements, and mitigation. Journal of Materials Engineering and Performance, 1-21.
41. Huang, W., Hou, B., Pang, Y., & Zhou, Z. (2006). Fretting wear behavior of AZ91D and AM60B magnesium alloys. Wear, 260(11-12), 1173-1178.
42. Kim, J. J., Kim, D. H., Shin, K. S., & Kim, N. J. (1999). Modification of Mg2Si morphology in squeeze cast Mg-Al-Zn-Si alloys by Ca or P addition. Scripta Materialia, 41(3), 333-340.
43. Guo, E. J., Ma, B. X., & Wang, L. P. (2008). Modification of Mg2Si morphology in Mg–Si alloys with Bi. Journal of Materials Processing Technology, 206(1-3), 161-166.
44. Wang, H. Y., Jiang, Q. C., Ma, B. X., Wang, Y., Wang, J. G., & Li, J. B. (2005). Modification of Mg2Si in Mg–Si alloys with K2TiF6, KBF4 and KBF4+ K2TiF6. Journal of Alloys and Compounds, 387(1-2), 105-108.

45. Qin, Q. D., Li, W. X., Zhao, K. W., Qiu, S. L., & Zhao, Y. G. (2010). Effect of modification and aging treatment on mechanical properties of Mg2Si/Al composite. Materials Science and Engineering: A, 527(9), 2253-2257.
46. Xiong, W., Qin, X. Y., Kong, M. G., & Li, C. H. E. N. (2006). Synthesis and properties of bulk nanocrystalline Mg2Si through ball-milling and reactive hot-pressing. Transactions of Nonferrous Metals Society of China, 16(5), 987-991.
47. Qin, Q. D., Zhao, Y. G., Zhou, W., & Cong, P. J. (2007). Effect of phosphorus on microstructure and growth manner of primary Mg2Si crystal in Mg2Si/Al composite. Materials Science and Engineering: A, 447(1-2), 186-191.
48. Bo, R. E. N., Liu, Z. X., Zhao, R. F., Zhang, T. Q., Liu, Z. Y., Wang, M. X., & Weng, Y. G. (2010). Effect of Sb on microstructure and mechanical properties of Mg2Si/Al-Si composites. Transactions of Nonferrous Metals Society of China, 20(8), 1367-1373.
49. Ahlatci, H. A. Y. R. E. T. T. İ. N. (2010). Production and corrosion behaviours of the Al–12Si–XMg alloys containing in situ Mg2Si particles. Journal of alloys and compounds, 503(1), 122-126.
50. Hadian, R., Emamy, M., Varahram, N., & Nemati, N. (2008). The effect of Li on the tensile properties of cast Al–Mg2Si metal matrix composite. Materials Science and Engineering: A, 490(1-2), 250-257.
51. Qin, Q. D., Zhao, Y. G., Liang, Y. H., & Zhou, W. (2005). Effects of melt superheating treatment on microstructure of Mg2Si/Al–Si–Cu composite. Journal of alloys and compounds, 399(1-2), 106-109.
52. Liao, L., Zhang, X., Wang, H., Li, X., & Ma, N. (2007). Influence of Sb on damping capacity and mechanical properties of Mg2Si/Mg–9Al composite materials. Journal of alloys and compounds, 430(1-2), 292-296.

53. Zhang, Z. M., Xu, C. J., Guo, X. F., & Jia, S. Z. (2008). Reciprocating extrusion of in situ Mg2Si reinforced Mg-Al based composite. Acta Metallurgica Sinica (English Letters), 21(3), 169-177.
54. Gan, W. M., Wu, K., Zheng, M. Y., Wang, X. J., Chang, H., & Brokmeier, H. G. (2009). Microstructure and mechanical property of the ECAPed Mg2Si/Mg composite. Materials Science and Engineering: A, 516(1-2), 283-289.
55. Wei, G. U. O., WANG, Q. D., Bing, Y. E., Hao, Z. H. O. U., & LIU, J. F. (2014). Microstructure and mechanical properties of AZ31–Mg2Si in situ composite fabricated by repetitive upsetting. Transactions of Nonferrous Metals Society of China, 24(12), 3755-3761.
56. Metayer, J., Bing, Y. E., Wei, G. U. O., Wang, Q. D., Hao, Z. H. O. U., & Mollet, F. (2014). Microstructure and mechanical properties of Mg–Si alloys processed by cyclic closed-die forging. Transactions of Nonferrous Metals Society of China, 24(1), 66-75.
57. Syukron, M., Ojima, M., Seman, A. A., Hussain, Z., & Koseki, T. (2016). Mechanical properties of 1.5 wt.% TiB2-added hypoeutectic Al-Mg-Si alloys processed by equal channel angular pressing. Procedia Chemistry, 19, 106-112.
58. Chegini, M., Shaeri, M. H., Taghiabadi, R., & Cheginy, S. (2021). Effect of equal channel angular pressing on microstructure and mechanical properties of thermally-homogenized Al–Mg2Si composites. Materials Chemistry and Physics, 259, 124200.
59. Guo, W., Wang, Q., Ye, B., Li, X., Liu, X., & Zhou, H. (2012). Microstructural refinement and homogenization of Mg–SiC nanocomposites by cyclic extrusion compression. Materials Science and Engineering: A, 556, 267-270.

60. El-Garhy, G., El Mahallawy, N., & Shoukry, M. K. (2021). Effect of grain refining by cyclic extrusion compression (CEC) of Al-6061 and Al-6061/SiC on wear behavior. Journal of Materials Research and Technology, 12, 1886-1897.
61. Charit, I., & Mishra, R. S. (2003). High strain rate superplasticity in a commercial 2024 Al alloy via friction stir processing. Materials Science and Engineering: A, 359(1-2), 290-296.
62. Kwon, Y. J., Shigematsu, I., & Saito, N. (2003). Mechanical properties of fine-grained aluminum alloy produced by friction stir process. Scripta materialia, 49(8), 785-789.
63. Sharma, S. R., Ma, Z. Y., & Mishra, R. S. (2004). Effect of friction stir processing on fatigue behavior of A356 alloy. Scripta Materialia, 51(3), 237-241.
64. Santella, M. L., Engstrom, T., Storjohann, D., & Pan, T. Y. (2005). Effects of friction stir processing on mechanical properties of the cast aluminum alloys A319 and A356. Scripta materialia, 53(2), 201-206.
65. Ma, Z. Y., Sharma, S. R., & Mishra, R. S. (2006). Effect of friction stir processing on the microstructure of cast A356 aluminum. Materials Science and Engineering: A, 433(1-2), 269-278.
66. Cavaliere, P., & De Marco, P. P. (2007). Friction stir processing of AM60B magnesium alloy sheets. Materials Science and Engineering: A, 462(1-2), 393-397.
67. Kang, S. H., Chung, H. S., Han, H. N., Oh, K. H., Lee, C. G., & Kim, S. J. (2007). Relationship between formability and microstructure of Al alloy sheet locally modified by friction stir processing. Scripta Materialia, 57(1), 17-20.
68. Charit, I., & Mishra, R. S. (2005). Low temperature superplasticity in a friction-stir-processed ultrafine grained Al–Zn–Mg–Sc alloy. Acta Materialia, 53(15), 4211-4223.

69. Chang, C., Du, X. H., & Huang, J. C. (2008). Producing nanograined microstructure in Mg–Al–Zn alloy by two-step friction stir processing. Scripta materialia, 59(3), 356-359.
70. Ni, D. R., Wang, D., Feng, A. H., Yao, G., & Ma, Z. Y. (2009). Enhancing the high-cycle fatigue strength of Mg–9Al–1Zn casting by friction stir processing. Scripta Materialia, 61(6), 568-571.
71. Zahmatkesh, B., Enayati, M. H., & Karimzadeh, F. (2010). Tribological and microstructural evaluation of friction stir processed Al2024 alloy. Materials & Design, 31(10), 4891-4896.
72. Joshi, S., Singh, R. C., & Chaudhary, R. (2019). Effect of rotational speed in friction stir processing on the microstructural and mechanical characteristics of cast AS21A magnesium alloy. Materials Research Express, 6(5), 056554.
73. Gultekin, D., Uysal, M., Aslan, S., Alaf, M., Guler, M. O., & Akbulut, H. (2010). The effects of applied load on the coefficient of friction in Cu-MMC brake pad/Al-SiCp MMC brake disc system. Wear, 270(1-2), 73-82.
74. Parthasarathi, N. L., Borah, U., & Albert, S. K. (2013). Correlation between coefficient of friction and surface roughness in dry sliding wear of AISI 316L (N) stainless steel at elevated temperatures. Computer Modelling and New Technologies, 17(1), 51-63.
75. Krishnan, C. S., Pokhrel, R., Mondal, A. K., & Masanta, M. (2020). Effect of temperature and applied load on sliding wear behaviour of AZ91D magnesium alloy. Materials Today: Proceedings, 26, 1136-1139.
76. Balamurugan, K. G., & Mahadevan, K. (2013). Investigation on the changes effected by tool profile on mechanical and tribological properties of friction stir processed AZ31B magnesium alloy. Journal of Manufacturing Processes, 15(4), 659-665.

77. Anasyida, A. S., Daud, A. R., & Ghazali, M. J. (2009). Dry sliding wear behaviour of Al-4Si-4Mg alloys by addition of cerium. International Journal of Mechanical and Materials Engineering, 4(2), 127-130.

78. Kato, K. (2011). Friction and wear of passive metals and coatings. In Tribocorrosion of Passive Metals and Coatings (pp. 65-99). Woodhead Publishing.

79. García-Rodríguez, S., Torres, B., Maroto, A., López, A. J., Otero, E., & Rams, J. (2017). Dry sliding wear behavior of globular AZ91 magnesium alloy and AZ91/SiCp composites. Wear, 390, 1-10.

80. Dwivedi, D. K. (2004). Sliding temperature and wear behaviour of cast Al–Si–Mg alloys. Materials Science and Engineering: A, 382(1-2), 328-334.